REPORT 1036

EXPERIMENTAL INVESTIGATION OF THE EFFECTS OF VISCOSITY ON THE DRAG AND BASE PRESSURE OF BODIES OF REVOLUTION AT A MACH NUMBER OF 1.5[1]

By Dean R. Chapman and Edward W. Perkins

SUMMARY

Tests were conducted to determine the effects of viscosity on the drag and base pressure of various bodies of revolution at a Mach number of 1.5. The models were tested both with smooth surfaces and with roughness added to evaluate the effects of Reynolds number for both laminar and turbulent boundary layers. The principal geometric variables investigated were afterbody shape and length-diameter ratio. For most models, force tests and base pressure measurements were made over a range of Reynolds numbers, based on model length, from 0.6×10^6 to 5.0×10^6. Schlieren photographs were used to analyze the effects of viscosity on flow separation and shock-wave configuration near the base and to verify the condition of the boundary layer as deduced from force tests. The results are discussed and compared with theoretical calculations.

The results show that viscosity effects are large and depend to a great degree on the body shape. The effects differ greatly for laminar and turbulent flow in the boundary layer, and within each regime depend upon the Reynolds number of the flow. Laminar flow was found up to a Reynolds number of 6.5×10^6 and may possibly exist to higher values.

The flow over the afterbody and the shock-wave configuration near the base are shown to be very much different for laminar than for turbulent flow in the boundary layer. The base pressure on bodies with boattailing is much higher with the turbulent layer than with the laminar layer, resulting in a negative base drag in some cases. The total drag characteristics at a given Reynolds number are affected considerably by the transition to turbulent flow. The foredrag of bodies without boattailing and of boattailed bodies for which the effects of flow separation are negligible can be calculated with reasonable accuracy by adding the skin-friction drag based upon the assumption of the low-speed friction characteristics to the theoretical wave drag.

For laminar flow in the boundary layer the effects of varying the Reynolds number were found to be large, approximately doubling the base drag in many cases. The total drag of the bodies without boattailing varied about 20 percent over the Reynolds number range investigated. For turbulent flow in the boundary layer, however, variations in Reynolds number had only a small effect on base drag and total drag.

INTRODUCTION

The effects of viscosity on the aerodynamic characteristics of bodies moving at low subsonic speeds have been known for many years and have been evaluated by numerous investigators. The effects of viscosity at transonic speeds have been investigated to a limited extent, and significant effects on the flow over airfoils have been reported by Ackeret (reference 1) and Liepmann (reference 2). The relative thoroughness of these two investigations has furnished a good start toward a satisfactory evaluation and understanding of the effects of viscosity in transonic flow fields. However, little is known about viscous effects at supersonic speeds.

The experiments reported in references 3, 4, and 5 have succeeded in evaluating the magnitude of the skin friction for supersonic flows in pipes and on rotating surfaces, but not for flow over a slender body or an airfoil.[2] Reference 6 contains a small amount of data on the effects of Reynolds number on the drag of a sphere and a circular cylinder; however, these data are not applicable to aerodynamic shapes which are practical for supersonic flight.

It has been sometimes assumed that the effects of viscosity are small and need be considered only when determining the magnitude of skin friction. In reviewing past data for the effects of viscosity it was found that in many reports, such as references 7 and 8, the model size was not stated, thereby rendering the calculation of Reynolds number and the evaluation of such tests quite difficult. Preliminary tests made during 1945 in the Ames 1- by 3-foot supersonic wind tunnel No. I, which is a variable-pressure tunnel, showed a relatively large effect of Reynolds number on the drag of bodies of revolution. The results of this cursory investigation were not reported because the magnitude of support interference was not known and because certain inaccuracies in the balance measurements were known to exist in the data taken at low tunnel pressures. An investigation of wing-body interaction at supersonic speeds has been conducted subsequently and the results presented in reference 9. Because of the support interference and the balance inaccuracies noted at low pressures the data presented therein on the effect of

[1] Supersedes NACA RM A7A31a, "Experimental Investigation of the Effects of Viscosity on the Drag of Bodies of Revolution at a Mach Number of 1.5" by Chapman, Dean R., and Perkins, Edward W., 1947. The principal results of various investigations conducted subsequent to 1947 which either pertain to or supplement the experiments described herein are indicated in footnotes.

[2] Subsequent to 1947 several investigations of skin friction have been conducted which indicate that at the supersonic Mach number of the present investigation the laminar and turbulent skin-friction coefficients for a flat plate are about 3- and 12-percent lower, respectively, than for low-speed flow at the same Reynolds number.

Reynolds number on the drag of smooth bodies are not sufficiently accurate throughout the range of Reynolds numbers for direct application to the conditions of free flight.

Since the effects of viscosity were known to be relatively large at the outset of this investigation, the purpose of the present research was made twofold. The primary purpose was to develop an understanding of the mechanism by which viscosity alters the theoretical inviscid flow over bodies of revolution at supersonic speeds, and the secondary purpose was to determine the magnitude of these effects for the particular bodies investigated. The experiments were conducted during 1946.

APPARATUS AND TEST METHODS

WIND TUNNEL AND INSTRUMENTATION

A general description of the wind tunnel and the principal instrumentation used can be found in reference 9. Included therein is a description of the strain-gage balance system employed for measuring aerodynamic forces and the schlieren apparatus which forms an integral part of the wind-tunnel equipment. In order to obtain accurate data at low as well as high tunnel pressures, a more sensitive drag gage was used in the present investigation than in the investigation of reference 9; however, all other details of the balance system were the same.

The tunnel total pressure, the static reference pressure in the test section, and the pressure in the air chamber of the balance housing were observed on a mercury manometer. Because the difference between the base pressure and the static reference pressure in the test section was ordinarily too small (only 0.5 cm. of mercury at low tunnel pressures) to be accurately read from a mercury manometer, a supplementary manometer using a fluid of lower specific gravity was employed. Because of its lower vapor pressure and its property of releasing little or no dissolved air when exposed to very low pressures, dibutyl phthalate, having a specific gravity of approximately 1.05 at room temperatures, was used as an indicating fluid in this manometer instead of the conventional light manometer fluids such as water and alcohol.

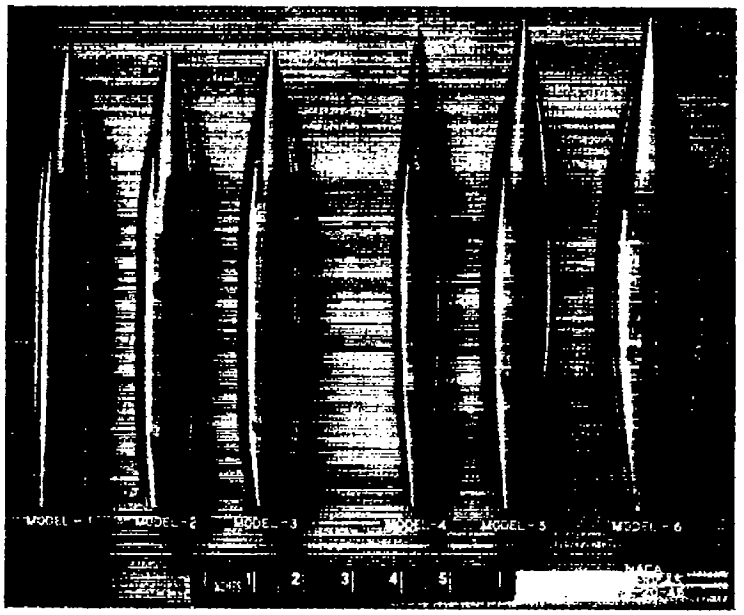

FIGURE 1.—Principal body shapes investigated.

MODELS AND SUPPORTS

Photographs of the models, which were made of aluminum alloy, are shown in figures 1 and 2, and their dimensions are given in figure 3. Models 1, 2, and 3 were each formed of a 10-caliber ogive nose followed by a short cylindrical section; they differ from one another only in the amount of boattailing. The shape of the ogive was not varied in this investigation because the flow over it is not affected appreciably by viscosity. Models 4, 5, and 6, which differ from from one another only in thickness ratio, were formed by parabolic arcs with the vertex at the position of maximum thickness. For convenience, some of the more important geometric properties of models 1 through 6 are listed in the following table:

Model	Frontal area A (sq in.)	Nose half angle (deg)	Length diameter ratio l/D	Base-area ratio A_B/A
1	1.227	18.2	7.0	1.00
2	1.227	18.2	7.0	.558
3	1.227	18.2	7.0	.348
4	.866	11.3	8.8	.191
5	1.758	15.9	6.2	.186
6	3.426	21.8	4.4	.187

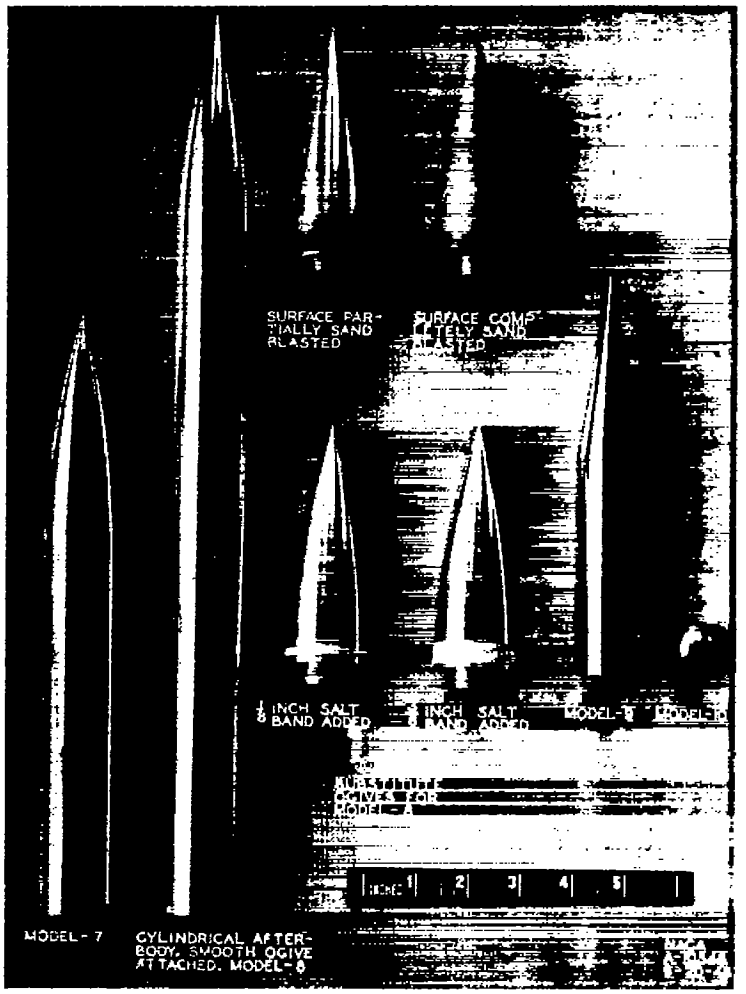

(a) Models used for boundary-layer tests and for comparison tests with other investigations.

FIGURE 2.—Special-purpose models.

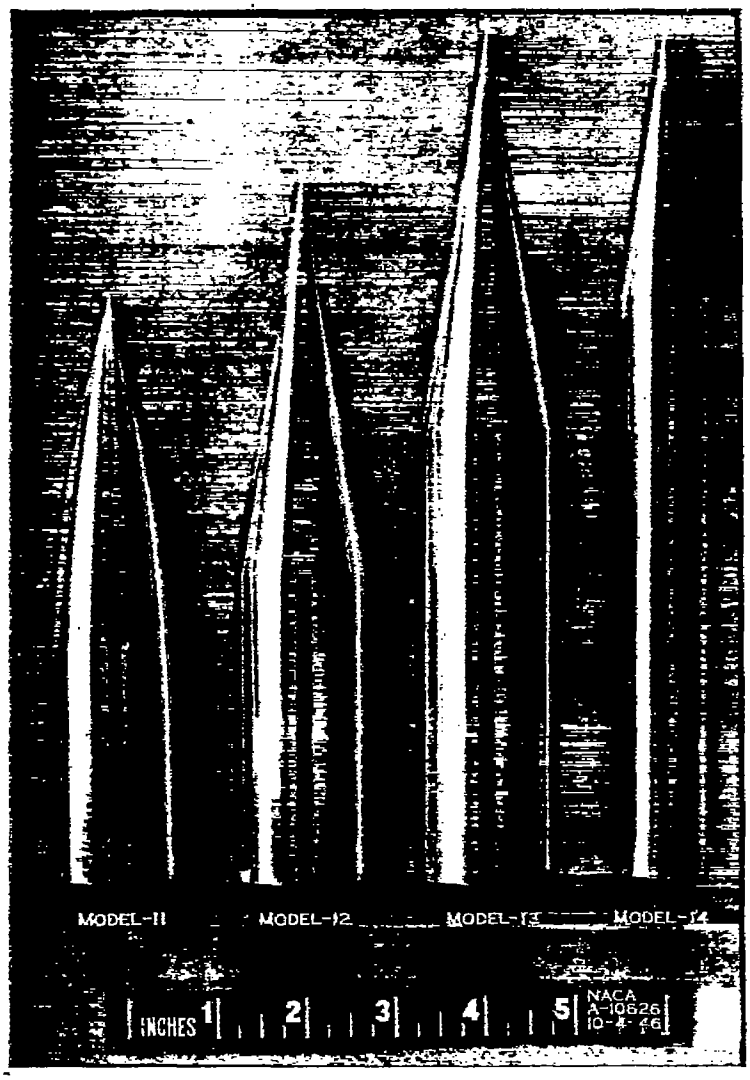

(b) Models used to evaluate effect of length-diameter ratio on base pressure.

FIGURE 2.—Concluded.

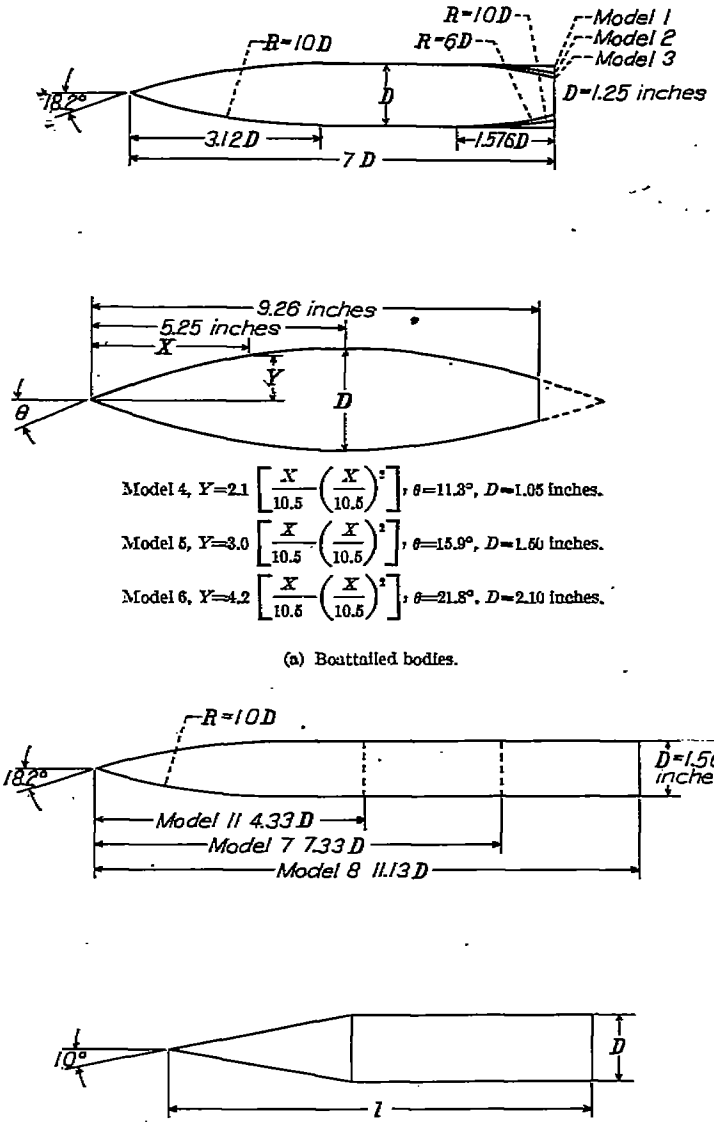

FIGURE 3.—Model dimensions.

In addition to the above-mentioned models, several other bodies were tested for certain specific purposes. Thus, models 7 and 8 were made unusually long so that the skin friction would be a large portion of the measured drag, thereby enabling the condition of the boundary layer to be deduced from force tests. Various substitute ogives, shown in figure 2 (a), were made interchangeable with the smooth ogive that is shown attached to the cylindrical afterbody of model 8. These ogives were provided with different types and amounts of roughness and could be tested either alone or with the long cylindrical afterbody attached. When the ogives were tested alone, a shroud of the same diameter as the ogive was used to replace the cylindrical afterbody. Model 9, a body with a conical nose, and model 10, a sphere of 1-inch diameter, were tested in order to compare the results of the present investigation with existing theoretical calculations and with the results of other experimental investigations. Models 11, 12, 13, and 14 were constructed to determine the effects of the length-diameter ratio for a fixed shape of afterbody. In all cases when a smooth surface was desired, the models were polished before testing to obtain a surface as free from scratches and machining marks as possible.

The models were supported in two different ways: by a rear support and by a side support, as shown in figure 4. The rear support used in the majority of the cases consisted of a sting which supported the model and attached to the balance beam. A thin steel shroud enclosed the sting and thereby eliminated the aerodynamic tare forces. Use of the rear support allowed force data, base pressure data, and schlieren photographs to be taken simultaneously. The side support which attached to the lower side of the model consisted of a 6-percent-thick airfoil of straight-side segments and 7° semiwedge angle at the leading and trailing edges. The side support was used to determine the effects of the axial variation in test-section static pressure on base pressure, and, in conjunction with a dummy rear support, to evaluate the effects of support interference.

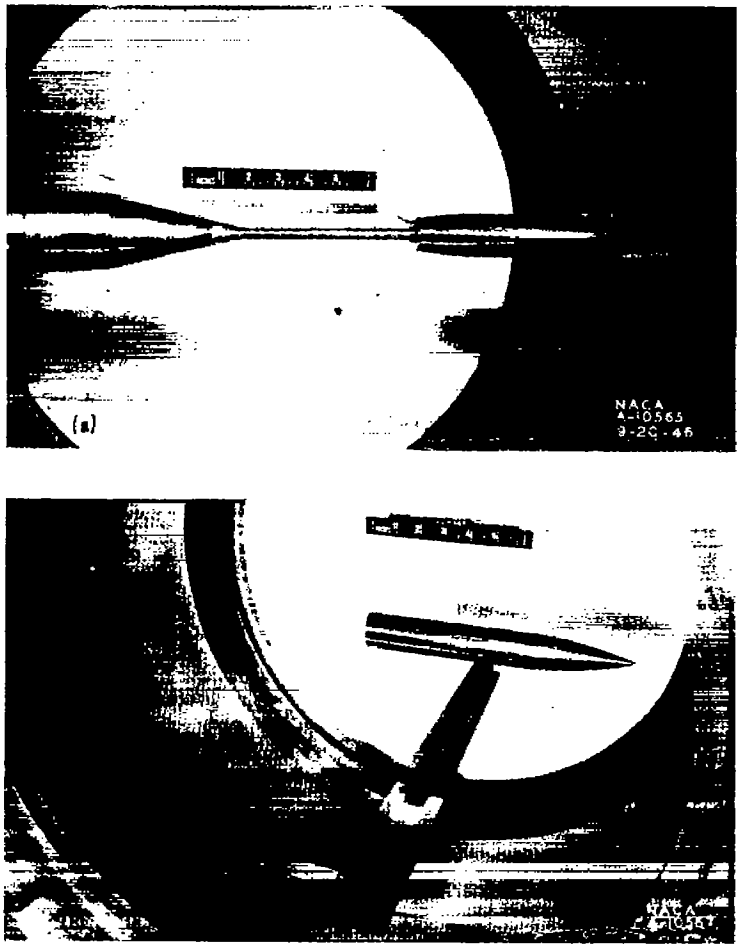

(a) Rear support.
(b) Side support.

FIGURE 4.—Typical model installations.

TEST METHODS

The tests were conducted at zero angle of attack in a fixed nozzle designed to provide a uniform Mach number of approximately 1.5 in the test section. For the positions occupied by the different models, the free-stream Mach number actually varied from 1.49 to 1.51. This is somewhat lower than the Mach number of the tests reported in reference 9, which were conducted farther downstream in the test section.

Before and after each run precautions were taken to test the pressure lines for leaks and the balance system for friction or zero shift. Each run was made by starting the tunnel at a low pressure, usually 3 pounds per square inch absolute, and taking data at different levels of tunnel stagnation pressure up to a maxiumm of 25 pounds per square inch absolute. Because of the lag in the manometer system, approximately 15 minutes at low pressures and 5 minutes at high pressures were allowed for conditions to come to equilibrium. The over-all variation in Reynolds number based on body length ranged from about 0.10×10^6 to 9.4×10^6. The specific humidity of the air usually was maintained below 0.0001 pound of water per pound of dry air, and in all cases was below 0.0003.

In general, each body was tested with a polished surface and then later with roughness added to fix transition. As illustrated in figure 2 (a), several different methods of fixing transition on a body in a supersonic stream were tried. The usual carborundum method employed in subsonic research was not used because of the danger of blowing carborundum particles into the tunnel-drive compressors. The method finally adopted was to cement a ⅛-inch-wide band of particles of table salt around the body. This method proved successful at all but the very low Reynolds numbers. On models 1, 2, 3, and 12, roughness was located ⅛ inch downstream of the beginning of the cylindrical section. On models 4, 5, and 6 the roughness was placed 4.5 inches from the nose and on model 8, ⅛ inch upstream of the beginning of the cylindrical afterbody. Models 7, 9, 10, 11, 13, and 14 were tested in the smooth condition only.

RESULTS

REDUCTION OF DATA

The force data included in this report have been reduced to the usual coefficient form through division by the product of the free-stream dynamic pressure and the frontal area of the body. In each case, conditions just ahead of the nose of a model are taken as the free-stream conditions.

The measurements of the pressure on the base of each model are referred to free-stream static pressure and made dimensionless through division by the free-stream dynamic pressure. Thus, the base pressure coefficient is calculated from the equation

$$P_b=\frac{p_b-p_\infty}{q_\infty} \tag{1}$$

where

P_b base pressure coefficient
p_b pressure acting on the base
p_∞ free-stream static pressure
q_∞ free-stream dynamic pressure

The dynamic pressure is calculated from the isentropic relationships. A small experimentally determined correction is applied for the loss in total pressure due to condensation of water vapor in the nozzle. The Reynolds number is based upon the body length and is calculated from the isentropic relationships using Sutherland's formula for the variation of viscosity with the temperature of the air.

It is convenient to consider the force due to the base pressure as a separate component of the total drag. Accordingly, the base drag is referred to the frontal area and in coefficient form is given by

$$C_{D_b}=-P_b\left(\frac{A_b}{A}\right) \tag{2}$$

where

C_{D_b} base drag coefficient
A_b area of base
A frontal area of the body

The foredrag is defined as the sum of all drag forces that act on the body surface forward of the base. Hence, the foredrag coefficient is given by

$$C_{D_f}=C_D-C_{D_b} \tag{3}$$

where C_D is the total drag coefficient and C_{D_f} the foredrag coefficient. The concept of foredrag coefficient is useful for several reasons. It is the foredrag that is of direct importance to the practical designer when the pressure acting on the base of a body is altered by a jet of gases from a power plant. Considering the foredrag as an independent compo-

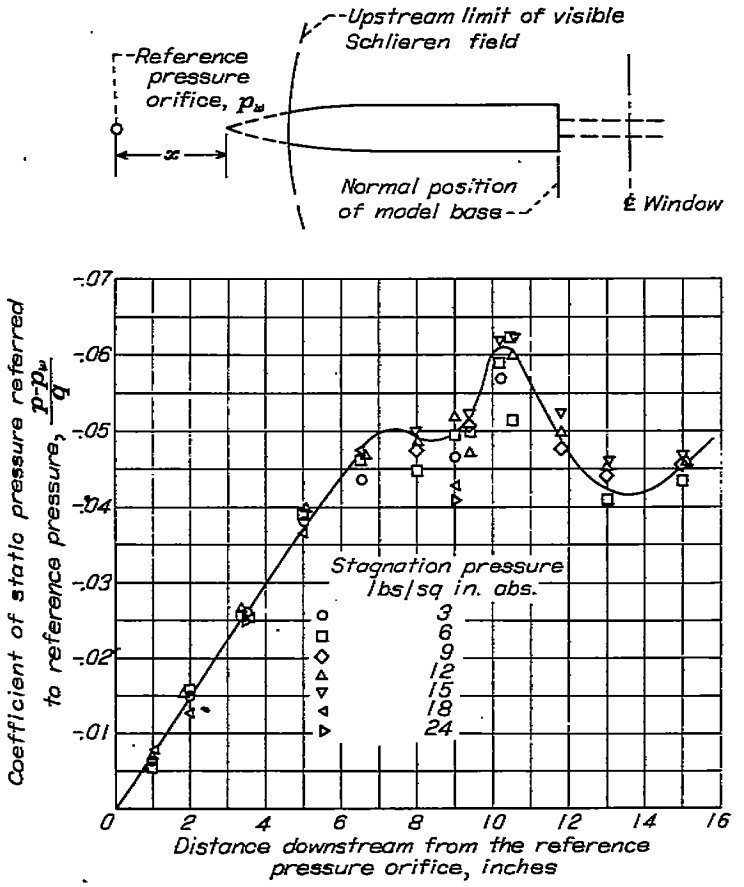

FIGURE 5.—Axial variation of the static pressure in the test section of the $M=1.5$ nozzle.

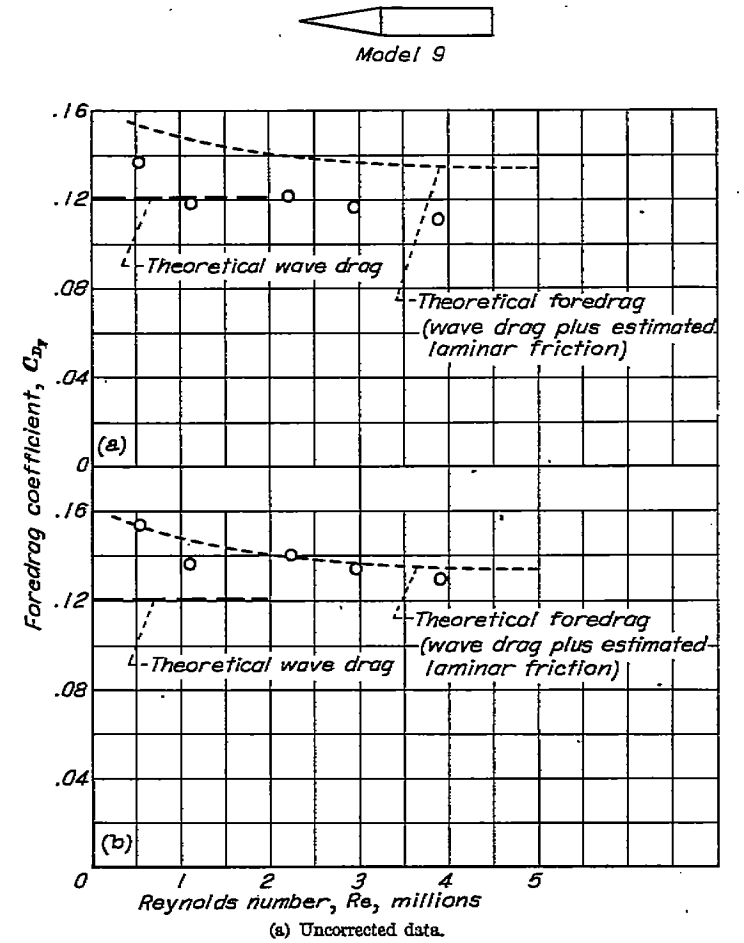

(a) Uncorrected data.
(b) Corrected data.

FIGURE 6.—Comparison of the foredrag coefficient of model 9 with and without corrections applied for the axial variation of the test-section static pressure.

nent of the total drag greatly simplifies the drag analysis of a given body. Finally, the foredrag, as will be explained later, is not affected appreciably by interference of the rear supports used in the investigation.

Since the nozzle calibration with no model present showed that the static pressure along the axis of the test section was not constant (fig. 5), the measured coefficients have been corrected for the increment of drag or pressure resulting from the axial pressure gradient. A detailed discussion of this correction is presented in appendix A, and the experimental justification is shown in figures 6 and 7.

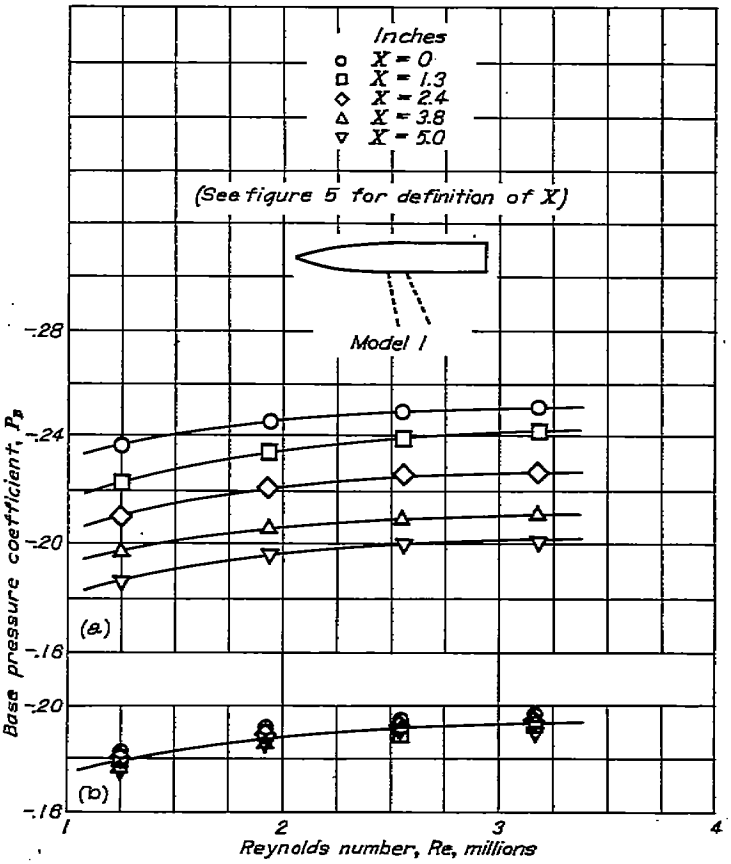

(a) Uncorrected data.
(b) Corrected data.

FIGURE 7.—Comparison of base pressure coefficients of model 1 measured at various positions along the tunnel axis, with and without corrections applied for the variation of test-section static pressure.

PRECISION

The table which follows lists the total uncertainty that would be introduced into each coefficient in the majority of the results if all of the possible errors that are known to exist in the measurement of the forces and pressures and the determination of free-stream Mach number and gradient corrections were to accumulate. Actually the errors may be expected to be partially compensating, so the probable inaccuracy is about half that given in the table. The sources and estimated magnitudes of the probable errors involved are considered at greater length in appendix B. The values in the following table are for the lowest and highest tunnel pressures and vary linearly in between. The table does not apply to data that are presented in figures 9 (b), 13, and 14. It also does not apply to models 4, 5, and 6 in figures 23 (a) and 29 (a) where the possible variation in the balance cali-

bration constant may increase the limits of error as discussed in appendix B.

Coefficient	Maximum value of error at lowest pressure	Maximum value of error at highest pressure
Total drag	±(2.4% plus 0.004)	±(1.1% plus 0.004)
Foredrag	±(1.6% plus 0.004)	±(0.6% plus 0.004)
Base pressure	±(1.6% plus 0.005)	±(0.5% plus 0.005)
Base drag	±[0.8% plus 0.005 (A_b/A)]	±[0.5% plus 0.005 (A_b/A)]

EFFECTS OF SUPPORT INTERFERENCE

Previous to the present investigation an extensive series of tests was conducted to determine the body shape and support combinations necessary to eliminate or evaluate the support interference. Based upon the results obtained, a summary of which appears in appendix C, it is believed that all the drag data presented herein for the models tested in the smooth condition are free from support interference effects with the exception of the data shown in figure 27. Also, for the models tested with roughness, the foredrag data are free from interference effects. However, an uncertainty in the base pressure coefficient exists which may vary from a minimum of ±0.005 to a maximum of ±0.015 for the different bodies. As a result, the base drag coefficients and total drag coefficients for the same test conditions are subject to a corresponding small uncertainty.

THEORETICAL CALCULATIONS

Although at present no theoretical method is available for calculating the base pressure and hence the total drag of a body, several methods are available which provide an excellent theoretical standard to which the experimental measurements of foredrag can be compared. In this report the theoretical foredrag is considered to be the sum of the theoretical wave drag for an inviscid flow and the incompressible skin-friction drag corresponding to the type of boundary layer that exists on the body.

A typical pressure distribution for the theoretical inviscid flow over one of the boattailed bodies tested in this investigation is shown in figure 8. For purposes of comparison the pressure distribution as calculated by the linear theory of von Kármán and Moore is included in this figure.

The wave drag of the cone-cylinder bodies was obtained from the theoretical flow over cones (references 10 and 11).[3] The wave drag for the ogive-cylinder bodies was calculated by the method of characteristics for rotationally symmetric supersonic flow as given in references 12 and 13. In accordance with the theoretical results of reference 14, the fluid rotation produced by the very small curvature of the head shock wave was neglected. For moderate supersonic Mach numbers this procedure is justified experimentally in reference 8, where the theoretical calculation using the method of characteristics as presented in reference 12 are shown to be in excellent agreement with the measured pressure distributions for ogives with cylindrical afterbodies.

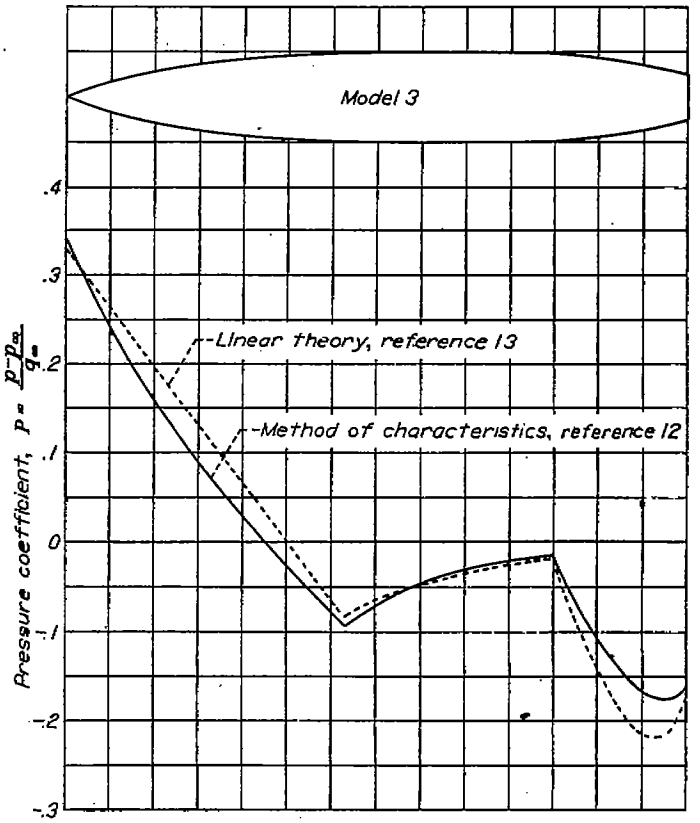

FIGURE 8.—Typical pressure distribution for a boattailed body at 1.5 Mach number.

An estimation of the skin-friction drag in any given case requires a knowledge of the condition of the boundary layer. The method used herein for laminar flow is as follows:

$$C_{D_f}=C_{f_{lam}}(A_F/A) \qquad (4)$$

where

C_{D_f} skin-friction drag coefficient for the model at the Reynolds number, Re, based on the full length of the model

$C_{f_{lam}}$ low-speed skin-friction coefficient for laminar boundary-layer flow over a flat plate at Re

A_F wetted area of the model forward of the base

A frontal area of the model

For the models with roughness added it is assumed that the disturbance of the boundary layer resulting from the salt band was sufficient to cause transition to a turbulent boundary layer to occur at the band. The skin-friction drag is estimated by means of the equation

$$C_{D_f}=C'_{f_{lam}}\left(\frac{A_{lam}}{A}\right)+C_{f_{turb}}\left(\frac{A_F}{A}\right)-C'_{f_{turb}}\left(\frac{A_{lam}}{A}\right) \qquad (5)$$

where

$C'_{f_{lam}}$ low-speed skin-friction coefficient for laminar boundary-layer flow at the effective Reynolds number, Re', based on the length of the model from the nose to the point where the salt band was added

A_{lam} wetted area of that portion of the model forward of the salt band

[3] In the original publication of the present investigation (1947) numerical values for the wave drag of the cones were based on the graphs of references 10 and 11. For the present report, however, slightly different numerical values are used which are based on more recent tabulated values of the surface pressure on cones in supersonic flow.

$C_{f_{turb}}$ low-speed skin-friction coefficient for turbulent boundary-layer flow over flat plate at the Reynolds number Re, based on the full length of the model

$C'_{f_{turb}}$ low-speed skin-friction coefficient for turbulent boundary-layer flow at the effective Reynolds number Re'

This method of calculation presumes that the fixed roughness was of such a nature as to cause the turbulent boundary-layer flow downstream of the point where the roughness was added to be the same as would have existed had the boundary-layer flow been turbulent all the way from the nose of the body.

DISCUSSION

FLOW CHARACTERISTICS

Before analyzing the effects of viscosity on the drag of the bodies of revolution, it is convenient to consider qualitatively the effects on the general characteristics of the observed flow. In so doing it is advantageous to consider first the condition of the boundary layer characterized by whether it is laminar or turbulent and then the effect of variation in Reynolds number on flow separation for each type of boundary layer. Once the effects of the Reynolds number and the condition of the boundary layer on flow separation are known, the observed effects on the shock-wave configuration at the base of the model are easily explained. Likewise, once the effects on flow separation and shock-wave configuration are known, the resulting effects of viscosity on the foredrag, base drag, and total drag are easily understood.

Condition of the boundary layer.—Since results observed at transonic speeds (references 1 and 2) have shown that the general flow pattern about a body depends to a marked degree on the type of boundary layer present, it might be expected that the boundary-layer flow at supersonic speeds also may be of primary importance in determining the over-all aerodynamic characteristics of a body. Consequently, the determination of the extent of the laminar boundary layer under normal test conditions is of fundamental importance.

In an attempt to determine the highest Reynolds number at which laminar flow exists on models tested in this investigation, a relatively long polished body (model 7) was tested from a low pressure up to the highest tunnel pressure obtainable. In this case, the diameter of the shroud which enclosed the rear support sting was made the same as the diameter of the body. The foredrag measurements on this model are shown in figure 9 (a). Since the skin friction is a relatively large portion of the measured foredrag, the condition of the boundary layer can be deduced from these force tests. The data indicate that the boundary layer on this body was still laminar up to the highest obtainable Reynolds number of 6.5×10^6. The computed foredrag data used for comparison are obtained by adding a laminar or turbulent skin-friction coefficient based on low-speed characteristics to the experimental wave drag of the ogival nose. This latter is determined by subtracting from the ogive foredrag coefficients the low-speed laminar skin-friction coefficients for the smooth ogive at the higher Reynolds numbers where the error, resulting from the assumption of the low-speed coefficients, is a small percent of the deduced wave drag. (The theoretical wave drag, based on the theoretical pressure distribution from the method of characteristics, is approximately 5 percent higher than the experimental wave drag.) Schlieren photographs from which the condition of the boundary layer may be observed are shown in figure 10. They confirm the previous finding by showing that transition does not occur on the body, but begins a short distance downstream from the base of the model, as indicated by arrow 1 in the photograph.

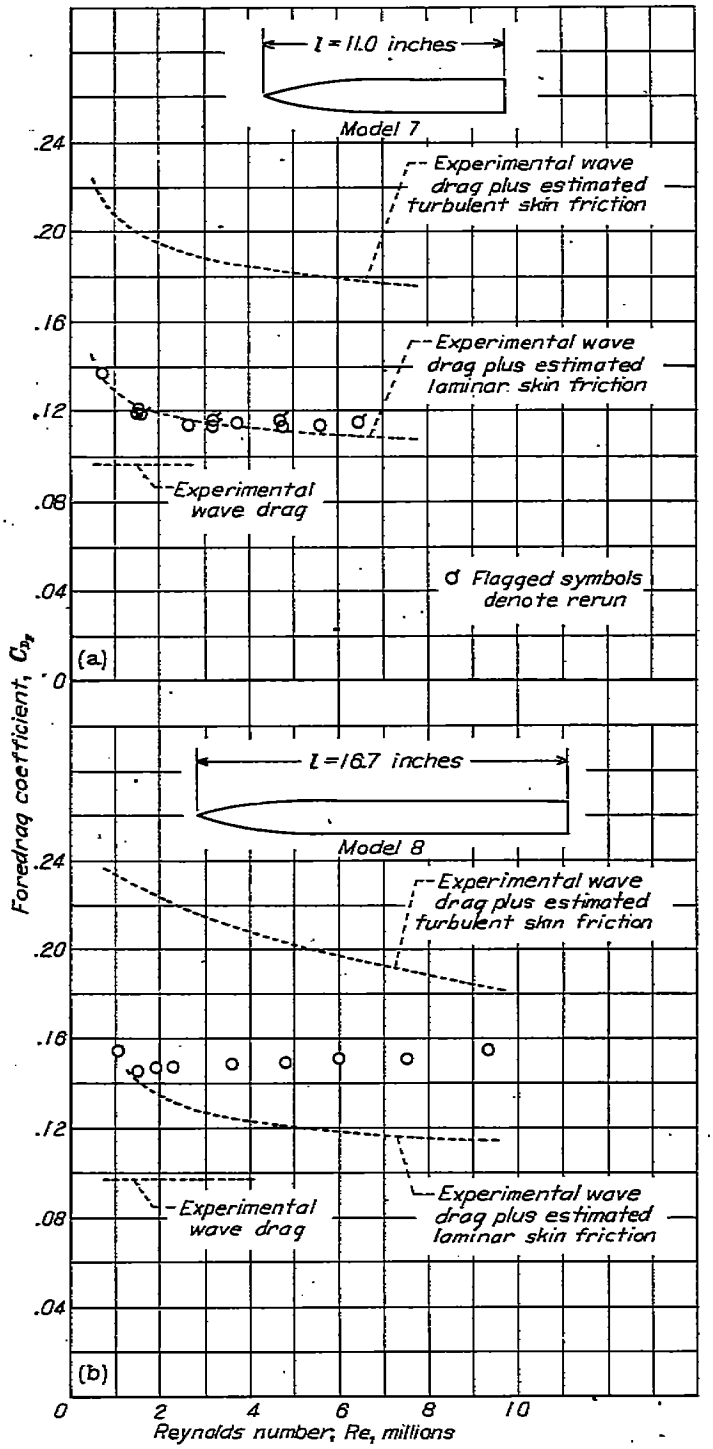

(a) Model 7.
(b) Model 8.

FIGURE 9.—Variation of foredrag coefficient with Reynolds number for models with long cylindrical afterbodies.

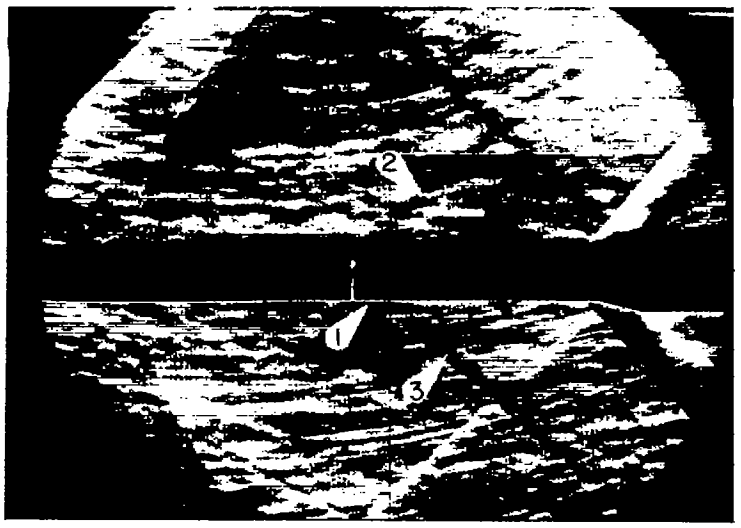

(a) Re=3.7×10⁶.

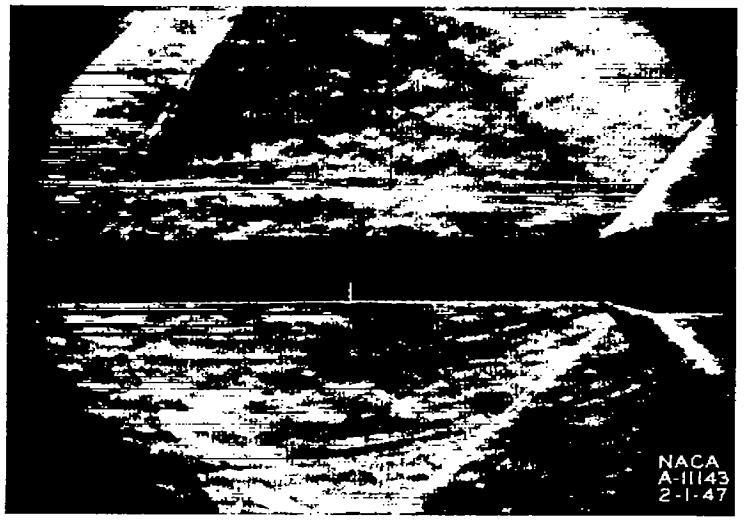

(b) Re=6.5×10⁶.

FIGURE 10.—Schlieren photographs showing laminar flow over the cylindrical afterbody of model 7 at two values of the Reynolds number. Knife edge horizontal.

A close examination of the photographs in figure 10 reveals that the beginning of transition (arrow 1) is located at the same point on the support shroud as the waves (arrows 2 and 3) which originate from a disturbance of the boundary layer. It was found by measurements on the schlieren photographs that the point of origin of these waves coincided with the intersection of the shroud and the reflected bow wave. This suggests that transition on the shroud is being brought about prematurely by the reflected bow waves. Additional evidence that this is not natural transition is obtained in noting from figure 10 that the point where transition begins does not move with a change in Reynolds number. If the model were longer than a critical length, which is about 11 inches for the conditions of the present tests, these reflected waves would strike the model somewhere on the afterbody and premature transition would be expected to affect the results. Figure 9 (b) shows the results of the measurements of foredrag on a 16.7-inch body (model 8), which is considerably longer than the critical length. These force data confirm the above conjecture by clearly indicating a partially turbulent boundary layer on the body even at Reynolds numbers as low as 2×10^6. The schlieren photographs of the flow over this body are presented in figure 11. It is seen that, in this case also, the transition to turbulent flow (arrow 1) is located at the same point as the waves (arrows 2 and 3) originating from the disturbance of the boundary layer by the reflected bow wave. Similary, an additional small wave (arrow 4) can be traced back to a disturbance of the boundary layer caused by a shock wave originating from an imperfect fit of the glass windows in the side walls.

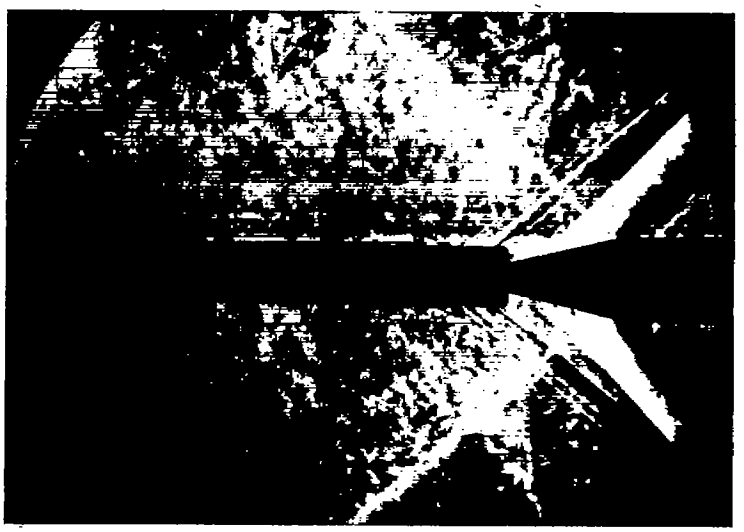

(a) Knife edge vertical.

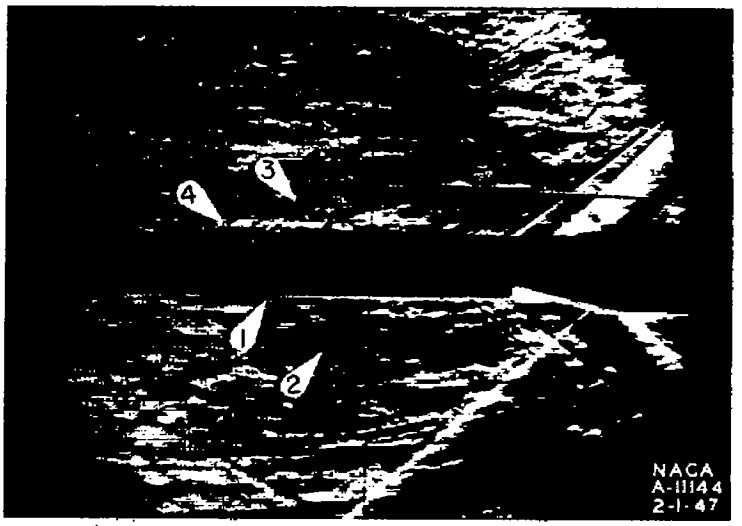

(b) Knife edge horizontal.

FIGURE 11.—Schlieren photograph showing premature transition on the cylindrical afterbody of model 8. Reynolds number 9.35×10⁶.

Although the maximum possible extent of laminar flow that may be expected on bodies of revolution cannot be determined on the basis of the present tests because of this interference from the reflected shock waves, the foregoing results show that, under the conditions of these tests, a laminar boundary layer exists over the entire surface of a smooth model about 11 inches long up to at least 6.5×10^6 Reynolds number. In comparison to the values normally encountered at subsonic speeds, a Reynolds number of 6.5×10^6 at first appears to be somewhat high for maintenance of laminar flow over a body, unless the pressure decreases in the direction

of the flow over the entire length of the body. The pressure distribution over model 7, shown in figure 12, has been determined by superimposing the pressure distribution which exists along the axis of the nozzle with no model present upon the theoretical pressure distribution calculated for model 7 by the method of characteristics. The resulting pressure distribution shows that the pressure decreases considerably along the ogive, but actually increases slightly along the cylindrical afterbody.

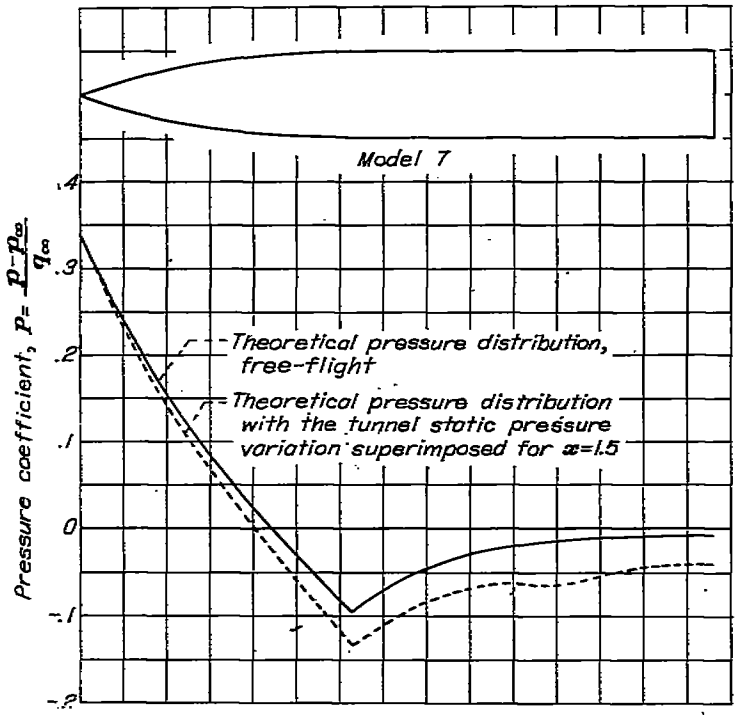

FIGURE 12.—Theoretical pressure distribution over the surface of model 7 at zero angle of attack and 1.5 Mach number.

An increase in the stability of the laminar boundary layer with an increase in Mach number has been indicated by the analysis of reference 15. With a given body shape, for which the pressure distribution changes with Mach number, an increase in stability with increasing Mach number has also been indicated for subsonic flows by the results of references 6 and 16 as well as by the experimental data given for airfoils in reference 15. The theoretical work of Lees (reference 17), however, indicates that the Reynolds number for neutral stability of laminar flow over an insulated flat plate decreases with an increase in Mach number.

It appears from the results of the present tests that any shock waves which originate from imperfections in the nozzle walls and disturb the boundary layer on a body can bring about transition prematurely. This may have some bearing on the results of the supersonic wind-tunnel tests conducted in the German wind tunnels at Kochel, since shock waves, ordinarily numbering about 15, are readily visible in various schlieren photographs. (See reference 18, for example.)

In order to cause the laminar boundary layer to become turbulent in the present investigation, an artifice such as adding roughness was necessary. In a supersonic stream, however, the addition of roughness to a body also increases the wave drag. The magnitude of the wave drag due to roughness was determined by testing with full diameter shrouding and no afterbody attached, first the smooth ogive, and then the ogives with various amounts and kinds of roughness added (fig. 2 (a)). The corresponding foredrag measurements are shown in figure 13. These data illustrate that little additional drag is attributable to roughness at the low Reynolds numbers where the boundary layer is relatively thick, but that an appreciable amount of wave drag is attributable to the roughness at the higher Reynolds numbers. For all subsequent results presented, the amount of drag caused by the artificial roughness has been subtracted from the measured data taken for the bodies tested with transition fixed. In order to calculate the amount of drag caused by the roughness for models of diameters different from the ogives tested, it was assumed that for any model the increment in drag coefficent attributable to the drag of the artificial roughness was inversely proportional to the diameter of the model at the station at which the roughness was applied.

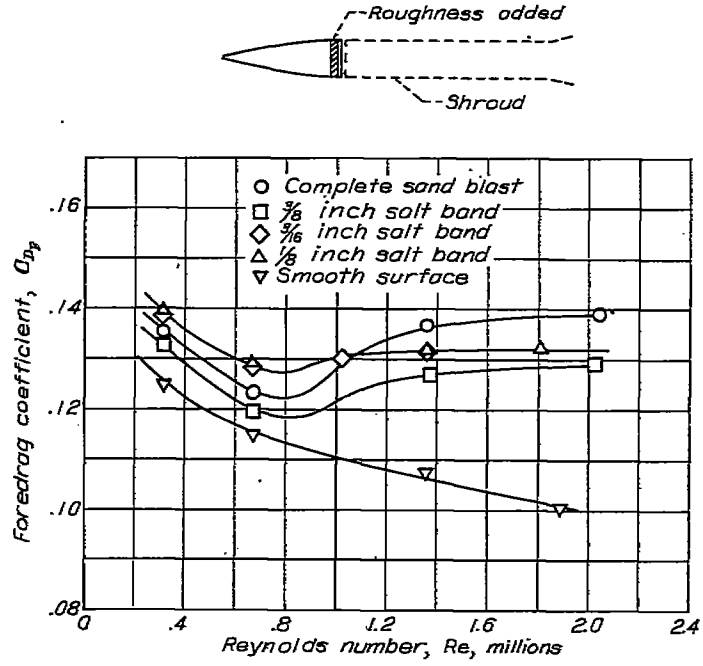

FIGURE 13.—Variation of foredrag coefficient with Reynolds number of the ogives with varying degrees of roughness added.

The foredrag measurements of model 8, which consists of a cylindrical afterbody with any one of the interchangeable ogives directly attached, are presented in figure 14. These data, from which the drag increment due to the added roughness has been subtracted as noted previously, show that the degree of roughness produced by sand blasting the surface of the ogive is insufficient to cause transition at low Reynolds numbers; whereas, the roughness produced by the 3/16-inch- or the ⅜-inch-wide salt band caused transition at all Reynolds numbers.

A vivid illustration of the turbulent character of the boundary layer on those bodies with roughness added is given by the schlieren photographs in figure 15. The boundary layer is best seen in the photograph taken with the knife edge horizontal. A comparison of these photographs with

those of laminar boundary layers (fig. 10, for example) illustrates how the condition of the boundary layer is apparent from schlieren photographs.

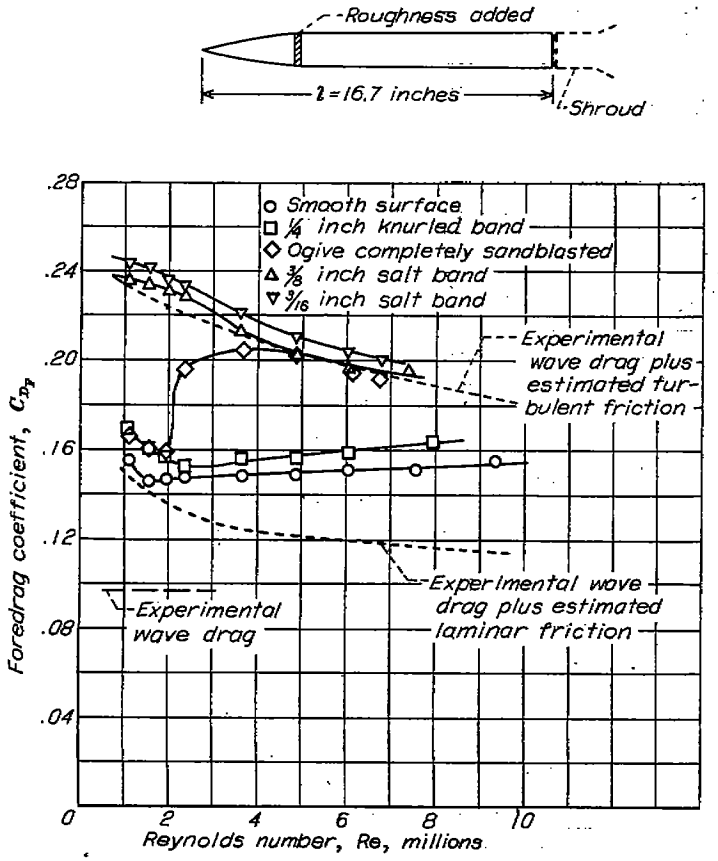

FIGURE 14.—Variation of foredrag coefficient with Reynolds number for model 8 with various amounts of roughness.

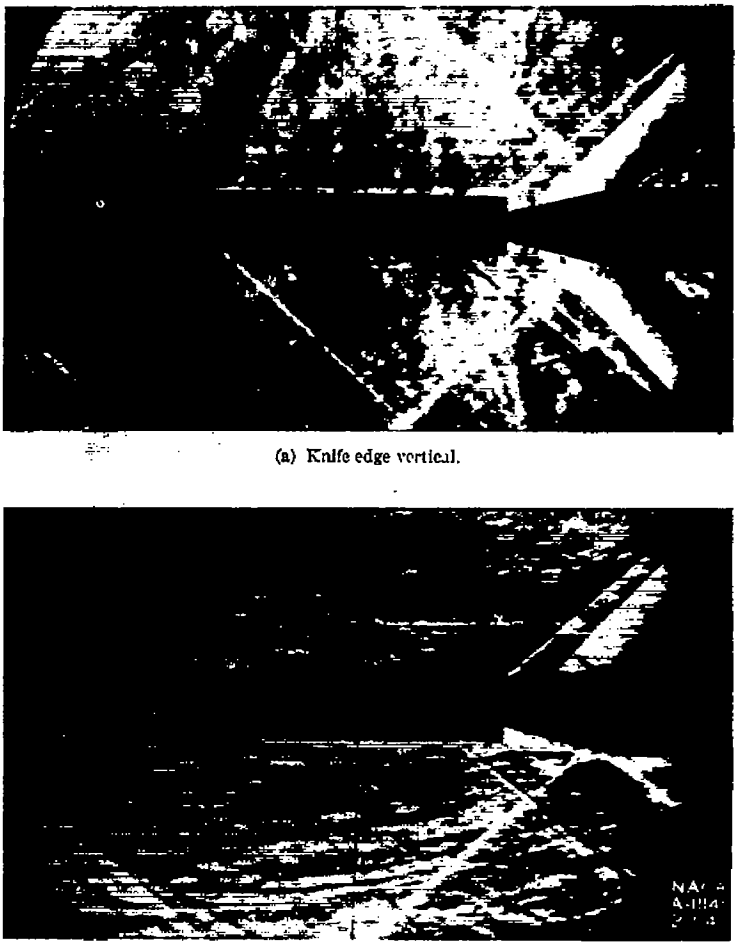

(a) Knife edge vertical.

(b) Knife edge horizontal.

FIGURE 15.—Schlieren photographs of model 8 with transition fixed. Reynolds number 7.2×10^6.

Flow Separation.—Changes in flow separation brought about by changing the boundary-layer flow from laminar to turbulent alter the effective shape of the body, the shock-wave configuration, and also the drag. It is therefore essential to consider the effects on flow separation of both the condition of the boundary layer and the Reynolds number.

The location and degree of separation of the laminar boundary layer for the boattailed bodies tested in the smooth condition varied noticeably with the Reynolds number of the flow. The schlieren photographs of model 6 in figure 16 are typical of this effect. Additional photographs, presented in figure 17, illustrate the same phenomena in the flow over models 2, 3, and 10, each at two different Reynolds numbers. In each case, as the Reynolds number of the flow is increased, the separation decreases, the convergence of the wake increases, and the trailing shock wave moves forward.

Separation of an apparently laminar boundary layer at supersonic speeds has been pointed out previously by Ferri in reference 19 for the two-dimensional flow over the surface of curved airfoils. The schlieren photographs of Ferri indicated that a shock wave formed at the point of laminar separation. On the other hand, the schlieren pictures of the flow fields for the bodies of revolution tested in the present investigation, show no definite shock wave accompanying separation except for the sphere (fig. 17) in which case the shock wave is very weak. It may be concluded, therefore, that a separation of the laminar boundary layer is not necessarily accompanied by a shock wave at supersonic speeds. The same conclusion for transonic flows has been drawn in reference 2.

In order to analyze more closely the details of the flow separation, the pressure distribution along the streamline just outside of the separated boundary layer was calculated for several flow conditions over models 3 and 6. The calculations were made using the method of characteristics and by obtaining the contour of the streamline just outside the separated boundary layer from enlargements of the schlieren photographs. Typical results from these calculations for model 3 are presented in figure 18. It is seen that the pressure on the outside of the boundary layer is approximately constant downstream of the point of separation as is characteristic along the boundary of a dead-air region. The pressure along the line of separation can be expected to be approximately equal to that in the dead-air region, and hence, equal to the base pressure. A comparison of the calculated values of the average pressure in the dead-air region with the measured values of the base pressure for several

conditions of flow over models 3 and 6 is given in the following table:

Model	Reynolds number	Calculated pressure coefficient of dead-air region	Measured base pressure coefficient
3	0.6×10^6	−0.06	−0.06
3	2.0×10^6	−.11	−.12
6	$.6\times10^6$	−.10	−.11
6	1.5×10^6	−.13	−.13

The preceding results indicate that under certain conditions the base pressure for laminar flow over highly boattailed bodies is directly related to the separation phenomenon which occurs forward of the base. This suggests that, if a means can be found to control the separation, the base pressure also can be controlled.

The theoretical pressure distributions on models 4 and 5 are similar to the pressure distribution on model 6, which is shown in figure 19. In each case the pressure in inviscid flow would decrease continually along the direction of flow upstream of the observed position of laminar separation. For subsonic flow this condition ordinarily would be termed favorable and separation would not be expected. Further research on this subject appears necessary in order to gain a satisfactory understanding of the observed results.

The findings of previous investigations of low-speed flows indicate that if a boundary layer which is normally laminar over the afterbody is made turbulent by either natural or artificial means, the resistance to separation is increased greatly. The tests on models 2, 3, 4, 5, and 6 with roughness added show clearly that this is also the case in supersonic flows. The two schlieren photographs presented in figure 20 were taken of model 6 with and without roughness added and are typical of this effect. A comparison of the two

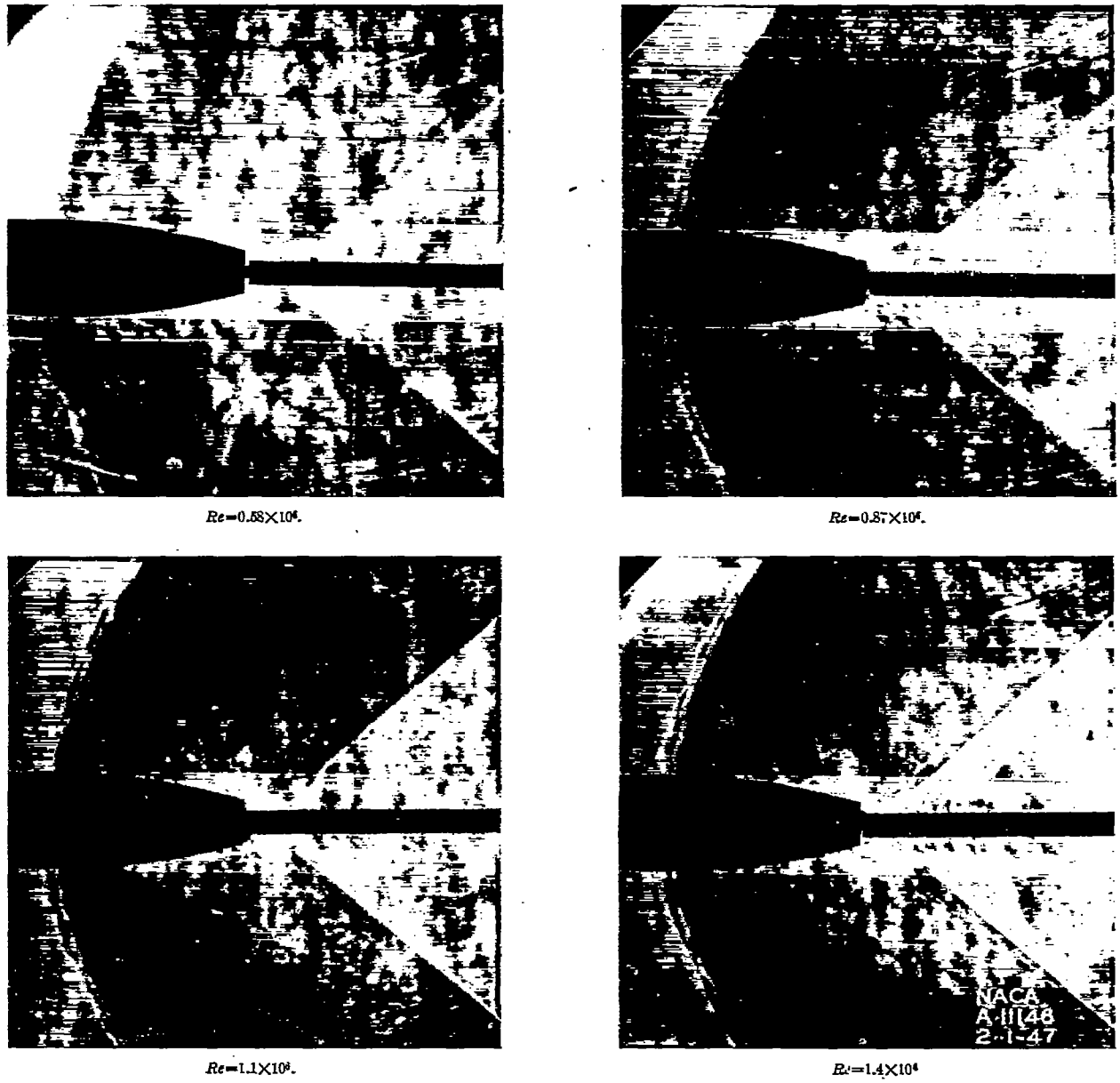

Re=0.58×10⁶. Re=0.87×10⁶.

Re=1.1×10⁶. Re=1.4×10⁶

FIGURE 16.—Schlieren photographs showing the effect of Reynolds number on laminar separation for model 6. Knife edge vertical.

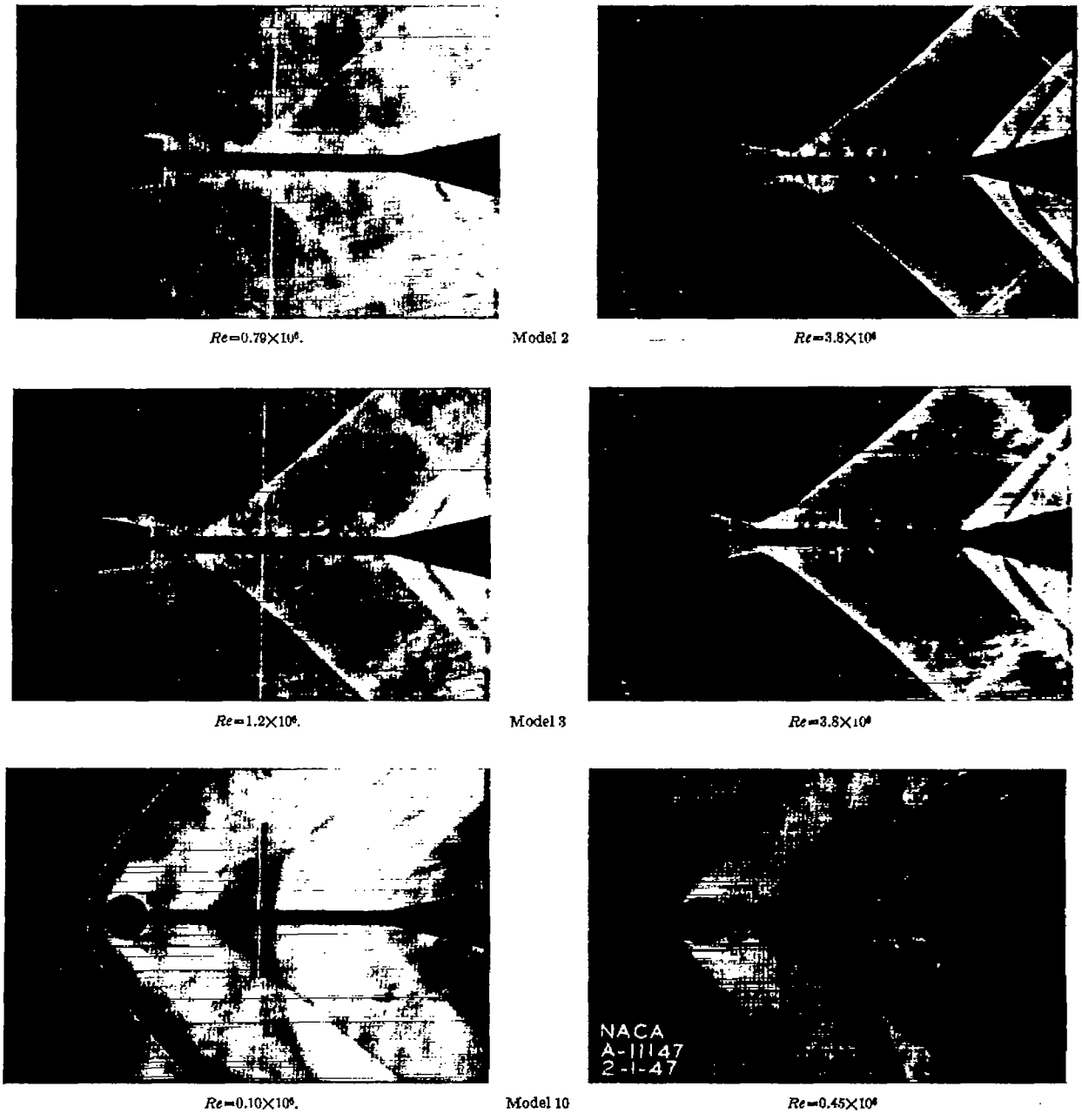

Re=0.79×10⁶. Model 2 Re=3.8×10⁶

Re=1.2×10⁶. Model 3 Re=3.8×10⁶

Re=0.10×10⁶. Model 10 Re=0.45×10⁶

FIGURE 17.—Schlieren photographs showing the effect of Reynolds number on laminar separation for models 2, 3 and 10. Knife edge vertical.

photographs shows that, without roughness added, separation occurs near the point of maximum thickness, but if transition is fixed ahead of this point the separation point moves downstream close to the base.

Shock-wave configuration.—It is to be expected that the changes in flow separation due to changes in the condition of the boundary layer and in the Reynolds number of the flow will bring about changes in the shock-wave configuration at the base of a body. The schlieren photographs of figures 16 and 17, which show how the laminar separation decreases and the convergence of the wake increases as the Reynolds number is increased, also show that these phenomena are accompanied by a forward motion of the trailing shock wave. In general, as long as the boundary layer is laminar, the trailing shock wave moves forward as the Reynolds number increases, but no major change in the shock-wave configuration takes place.

The shock-wave configuration on a boattailed body with a turbulent boundary layer, however, is very much different from the configuration with a laminar layer, as is illustrated by the schlieren photographs of model 6, shown in figure 20. Such configuration changes due to the transition to turbulent boundary-layer flow correlate quite well with the angle β that the tangent to the surface just ahead of the base makes with the axis of symmetry. Figure 21 shows the changes in shock-wave configuration for models 1 through 6 arranged in order of increasing angle β. It is seen that, on the boattailed bodies with a small angle β, the transition to a turbulent boundary layer is accompanied by the appearance of a weak shock wave originating at the base of the body (models 4 and 2). For bodies with larger boattail angles (model 5) the strength of this wave, hereafter termed the "base shock wave," increases until it is approximately as strong as the original trailing shock wave. For even larger boattail angles,

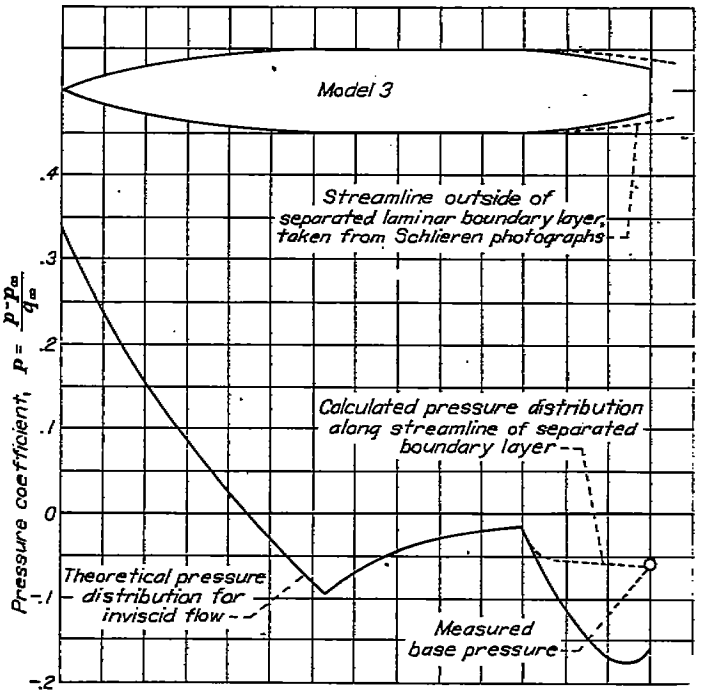

FIGURE 18.—Calculated pressure distribution for model 3 at a Reynolds number of 0.6×10^6.

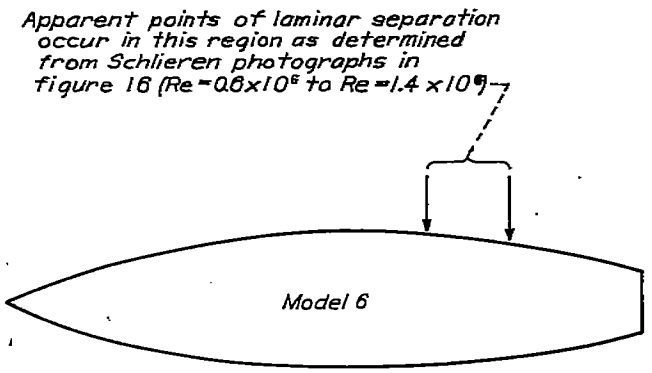

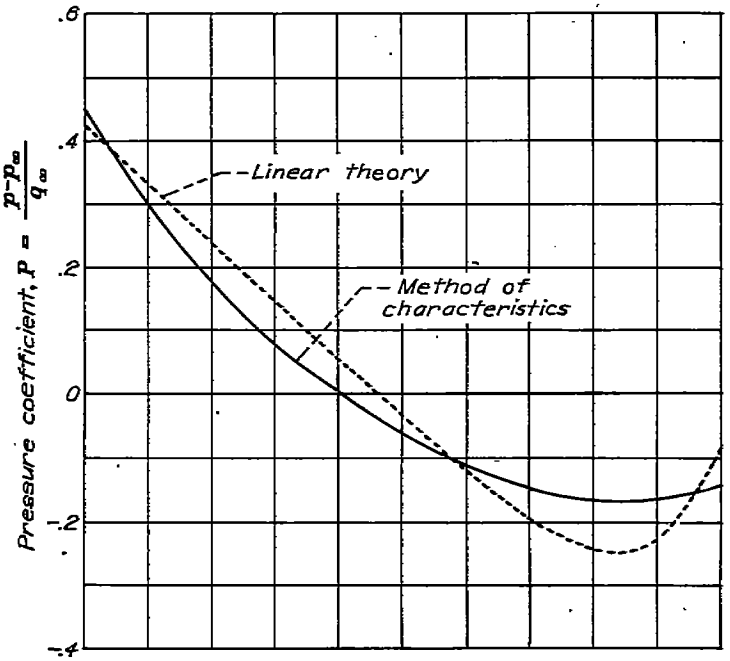

FIGURE 19.—Calculated pressure distribution on model 6.

(a) Laminar boundary layer, $Re=0.87\times10^6$.

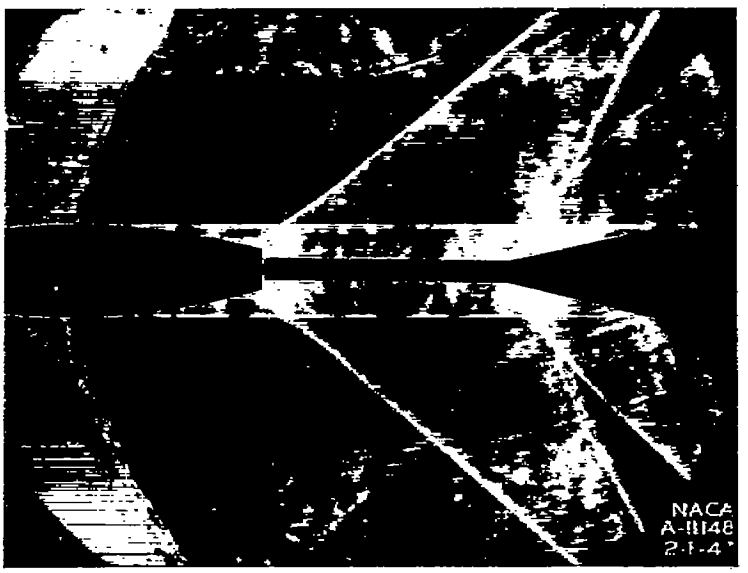

(b) Turbulent boundary layer, $Re=0.87\times10^6$.

FIGURE 20.—Schlieren photographs of model 6 illustrating the effect on flow separation of the condition of the boundary layer.

the base shock wave becomes more distinct, and eventually is the only appreciable shock wave existing near the base of the body (models 3 and 6).[4] In such a case, the compression through the base shock wave occurs forward of the base. This, as will be shown later, greatly increases the base pressure and decreases the base drag.

Compared to the phenomena observed with a laminar boundary layer (fig. 16), changes in the Reynolds number for a body with a turbulent boundary layer do not alter the shock-wave configuration to any significant extent, because the turbulent layer, even at low Reynolds numbers, ordinarily does not separate. This fact is evident in figure 22, which shows the schlieren photographs of model 3 at different Reynolds numbers with roughness added. No apparent change in the flow characteristics takes place as the Reynolds number is increased. With a turbulent boundary layer,

[4] Subsequent experiments with turbulent flow on model 3 at higher Mach numbers have shown that the base shock wave also exists at a Mach number of 2.0, but virtually disappears at a Mach number of 3.0 and higher.

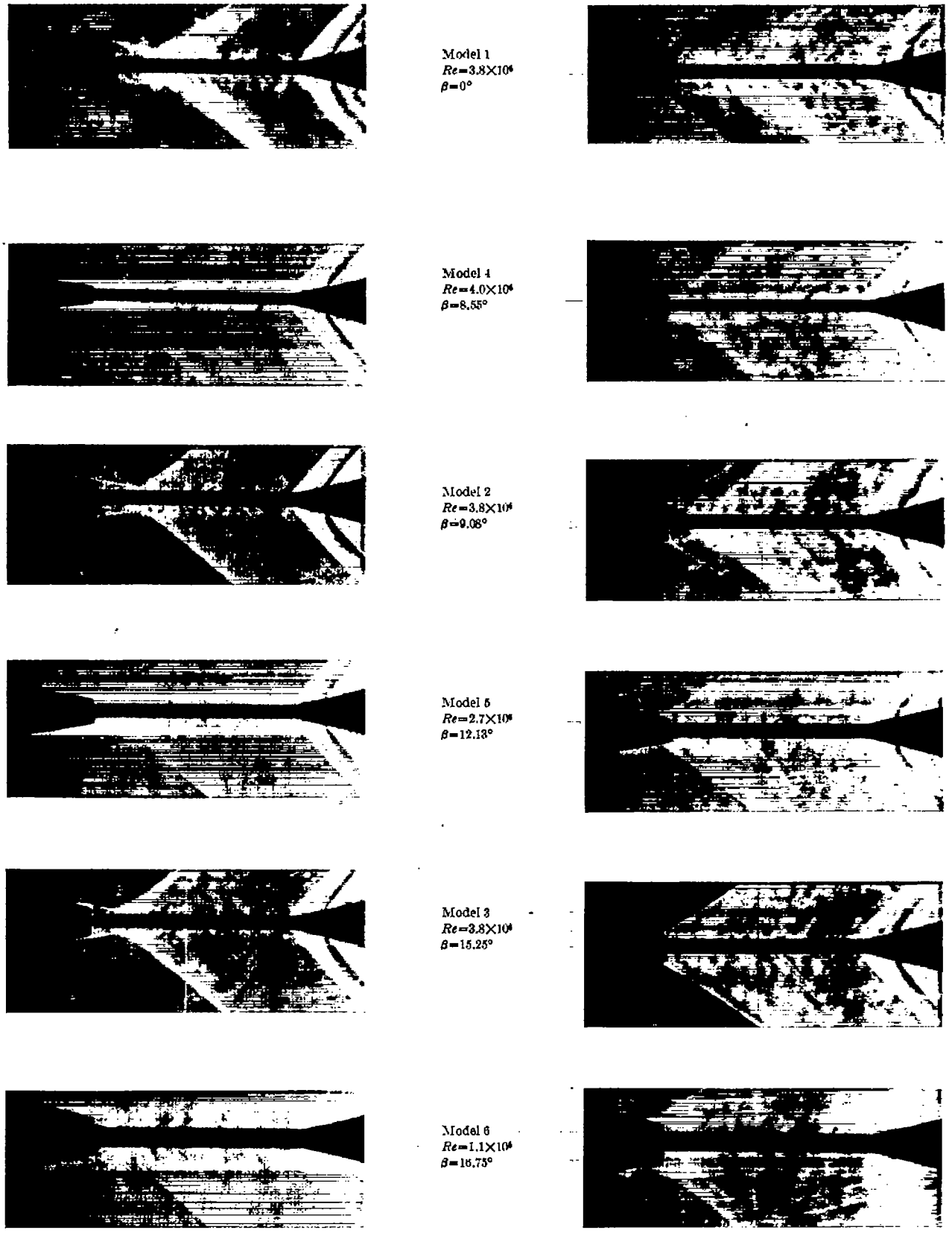

FIGURE 21.—Schlieren photographs showing the effect of turbulent boundary layer on shock-wave configuration at base of models 1, 2, 3, 4, 5 and 6. Knife edge vertical.

therefore, the effect on base drag of varying the Reynolds number may be expected to be much less than with a laminar layer.

ANALYSIS OF THE DRAG DATA

The qualitative effects of viscosity on flow separation and on shock-wave configuration, which have been discussed in the preceding sections, provide the physical basis for understanding the effects of varying the Reynolds number and changing the condition of the boundary layer on the drag coefficients of the various bodies tested.

Foredrag.—The foredrag coefficients of models 1 through 6 with laminar flow in the boundary layer are shown in figure 23 (a) as a function of the Reynolds number. These data show that, over the Reynolds number range covered in the tests, the foredrag of model 1 decreases about 20 percent, while that of model 6 increases about 15 percent. The foredrag of the other bodies does not change appreciably.

The reason the effects of Reynolds number vary considerably with different body shapes is clearly illustrated by a comparison of the measured foredrags with the theoretical foredrags. In figure 24 (a) the theoretical and measured values of foredrag are compared for model 1, which has no boattailing, and for model 3, which is typical of the boattailed models. From this comparison, it is seen that, as previously noted for other models without boattailing, the theoretical and experimental foredrags for model 1 are in good agreement. The decrease in foredrag with increasing Reynolds number for the bodies without boattailing is due entirely to the decrease in skin-friction coefficient. For model 3, which has considerable boattailing, the curves of figure 24 (a) show that the theoretical and experimental foredrags agree only at high Reynolds numbers. At the low Reynolds numbers the measured foredrags are lower than the theoretical values because of the separation of the laminar boundary layer as previously illustrated by the schlieren photographs in figures 16 and 17. With sep-

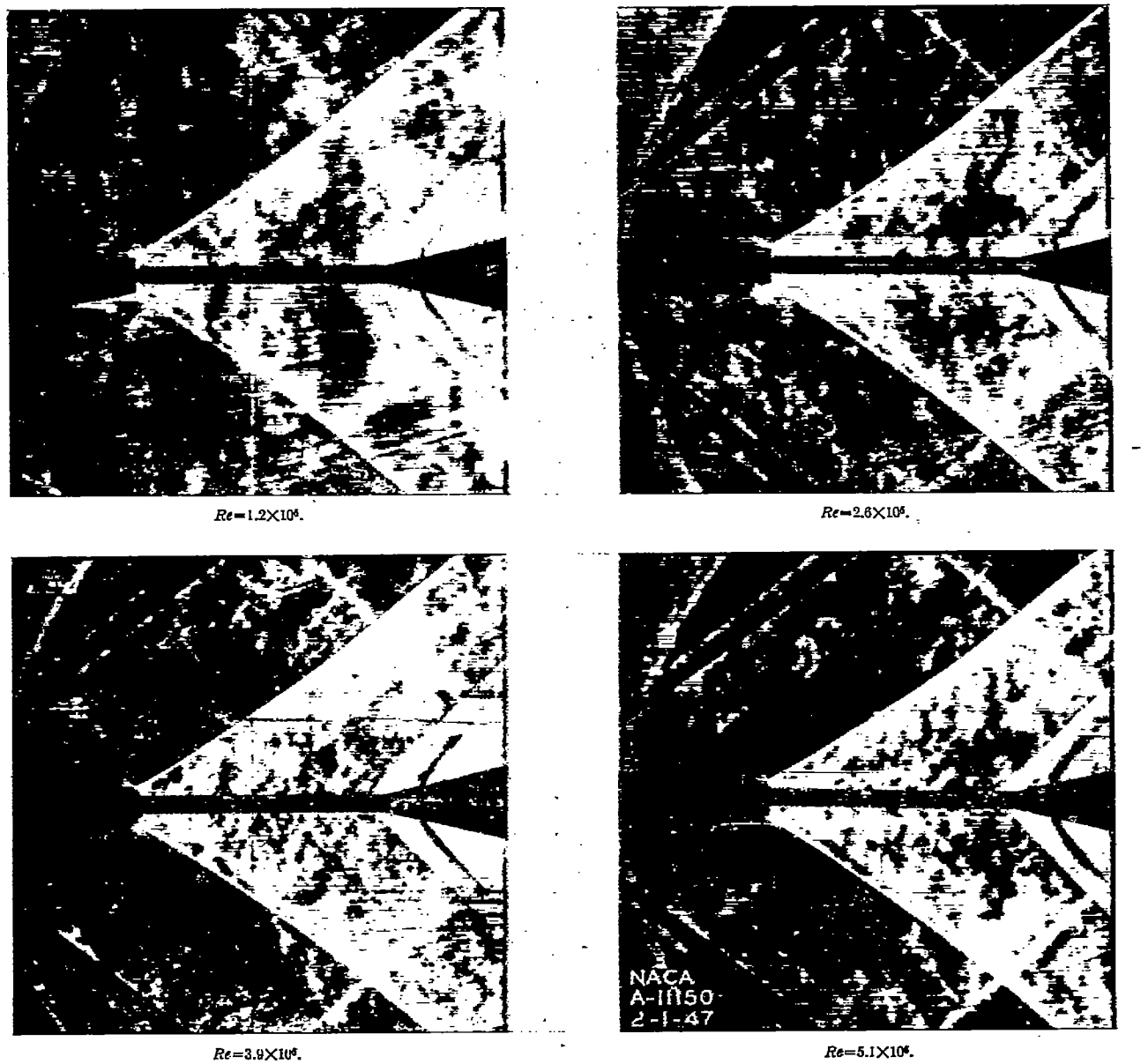

Re=1.2×10⁶. Re=2.6×10⁶. Re=3.9×10⁶. Re=5.1×10⁶.

FIGURE 22.—Schlieren photographs showing the absence of any effect of Reynolds number on the flow over the afterbody of model 3 with roughness added. Knife edge vertical.

aration, the flow over the boattail does not follow the contour of the body, and the pressure in the accompanying dead-air region is higher than it would be if the separation did not occur (fig. 18). This makes the actual foredrag lower than the theoretical value for a flow without separation. At the higher Reynolds numbers, the separation is negligible and the flow closely follows the contour of the body; hence, the theoretical and experimental foredrags agree. The reason for the approximately constant foredrag of models 2, 3, 4, and 5, therefore, is that the changes due to skin friction and flow separation are compensating. For model 6 with a smooth surface, the foredrag shown in figure 23 (a) rises rather rapidly at low Reynolds numbers because the separation effects for this relatively thick body (fig. 16) more than compensate for the changes in skin friction due to the variation of the Reynolds number.

Figure 23 (b), which shows the foredrag coefficients of model 1 through 6 with roughness added, indicates that the foredrag for all the bodies decreases as the Reynolds number increases above a Reynolds number of 1.75×10^6. This is to be expected, since with the change to turbulent boundary layer and consequent elimination of separation, the only factor remaining to influence the foredrag coefficients is the decrease of skin-friction coefficients with increase in Reynolds number. Below a Reynolds number of 1.75×10^6, however, the foredrag of all the models except model 1 increases with increasing Reynolds number. The cause of this somewhat puzzling behavior is apparent upon closer examination of the data.

Figure 24 (b) shows a comparison of the theoretical foredrags with the experimental values for models 1 and 3 with roughness added. The theoretical value for skin-friction drag was calculated assuming laminar flow up to the location of the roughness, and turbulent flow behind it. This value of drag was added to the theoretical wave drag to obtain the theoretical foredrag. It is seen from figure 24 (b) that for model 1 the curves of theoretical and experimental foredrag have the previously indicated trend of decreasing drag with increasing Reynolds number over the entire range. However, for model 3, which is typical of the boattailed bodies, the measured foredrag at low Reynolds numbers falls considerably below the theoretical value in the manner previously noted. The reason for this is evident from an examination of the schlieren photographs shown in figure 25, which were taken of the flow over models 3 and 6 with roughness added. They show that at the low Reynolds numbers a flow separation similar to that observed for the smooth body (fig. 16) occurs, and the resulting shock-wave configuration is characteristic of the configuration for a laminar boundary layer rather than that for a turbulent boundary layer. It appears that, at the low Reynolds numbers, the amount of roughness added does not cause transition far enough upstream of the point for laminar separation so that the free stream can provide the boundary layer with the necessary additional momentum to prevent separation. The portions of the drag curves in which the desired transition was not realized are shown dotted over the region in which separation was apparent from the schlieren pictures. For model 1, the schlieren photographs showed that at the low Reynolds numbers the amount of roughness added was

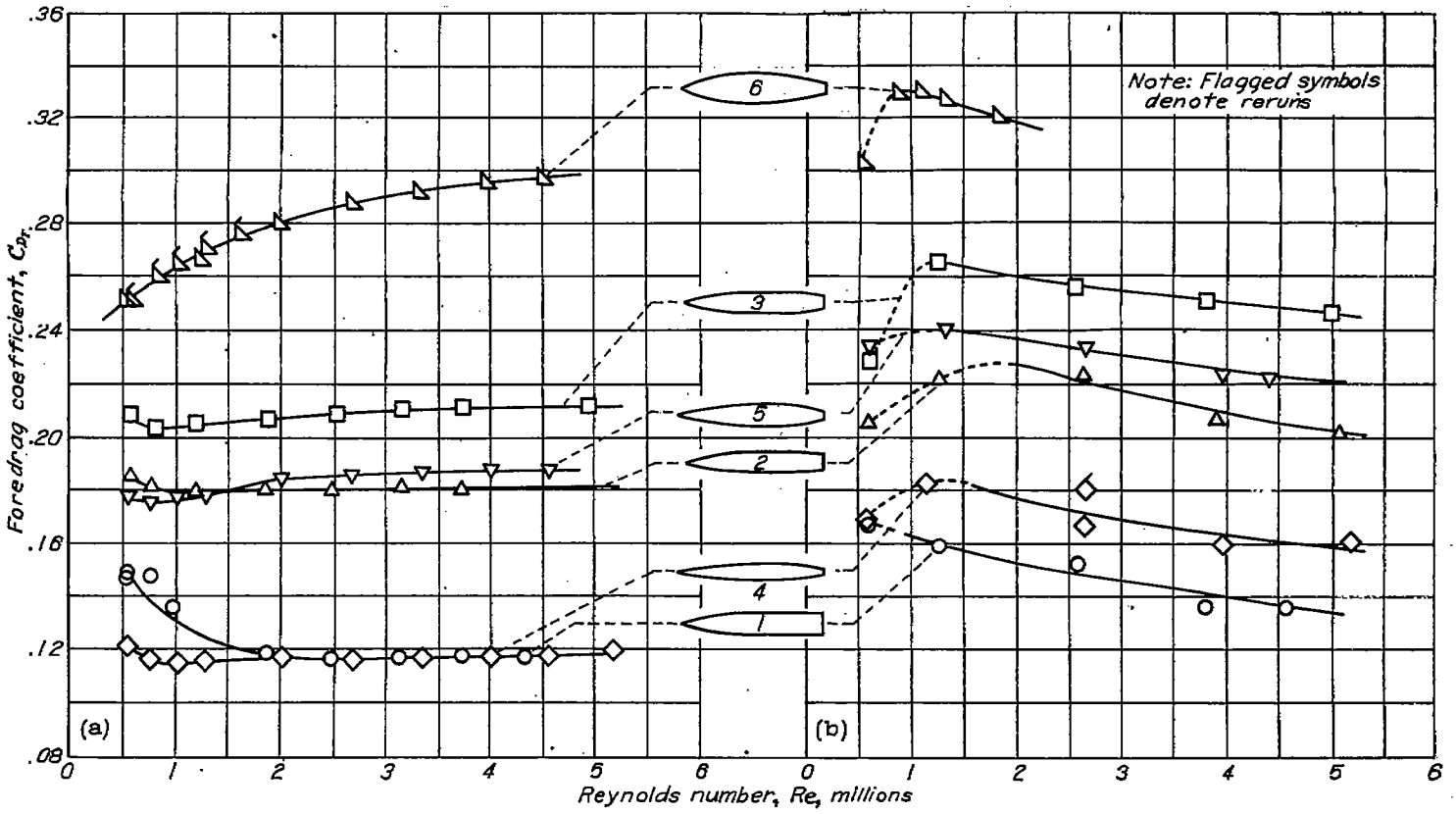

(a) Smooth condition. (b) Roughness added.

FIGURE 23.—Variation of foredrag coefficient for models 1, 2, 3, 4, 5 and 6 in the smooth condition and with roughness added.

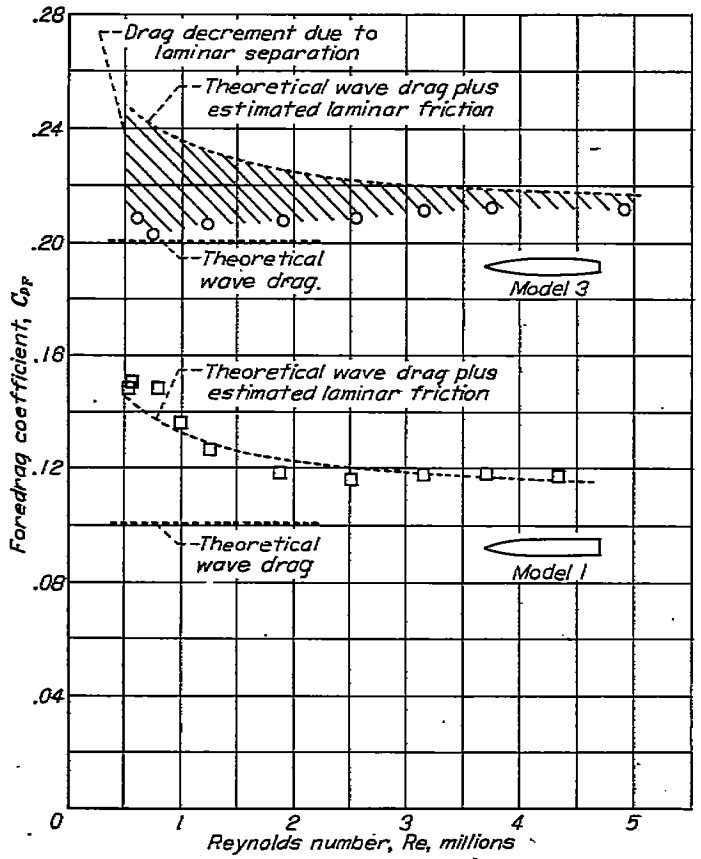

(a) Smooth condition.

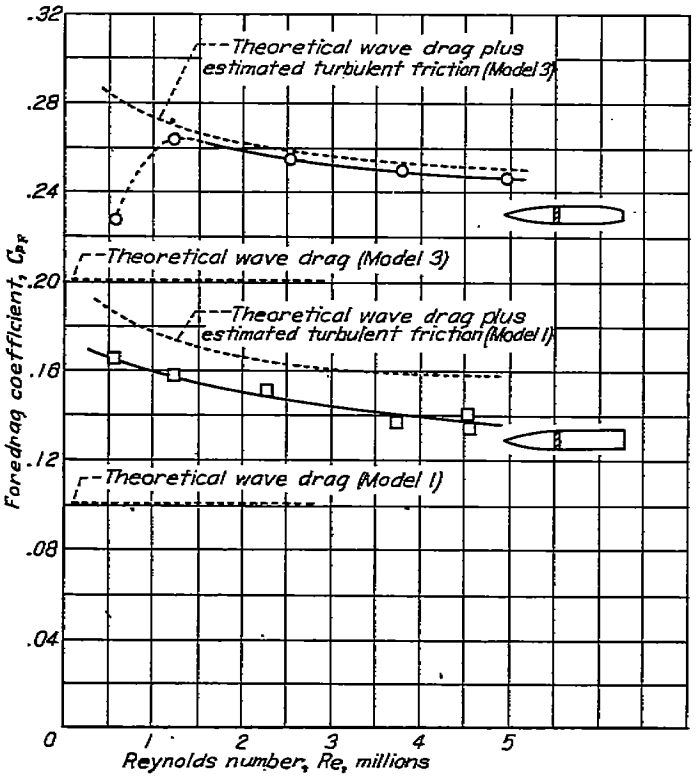

(b) Roughness added.

FIGURE 24.—Comparison of theoretical and experimental foredrag coefficients for models 1 and 3.

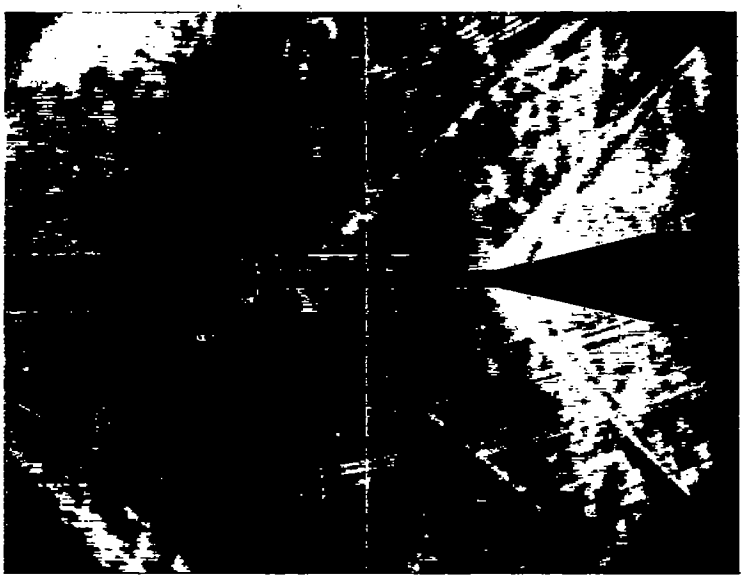

(a) Model 3, Re=0.58×10^6.

(b) Model 6, Re=0.62×10^6.

FIGURE 25.—Schlieren photographs at low Reynolds numbers of models 3 and 6 with roughness added. Knife edge vertical.

sufficient to effect transition some distance ahead of the base, although not immediately aft of the roughness.

The agreement between the experimental and the theoretical results obtained by the use of equations (4) and (5) indicates that, at a Mach number of 1.5 and in the range of Reynolds numbers covered by this investigation, the familiar low-speed skin-friction coefficients can be used with fair approximation to estimate drag due to skin friction at supersonic speeds.

A comparison of the curves of figures 23 (a) and 23 (b) shows that for a given body at a given value of the Reynolds number the foredrag with roughness added is consistently higher than the corresponding foredrag of the smooth-surfaced body. In the general case, this over-all increase in foredrag is attributable both to the increase in the skin-friction drag of the body and to the change in flow separation with

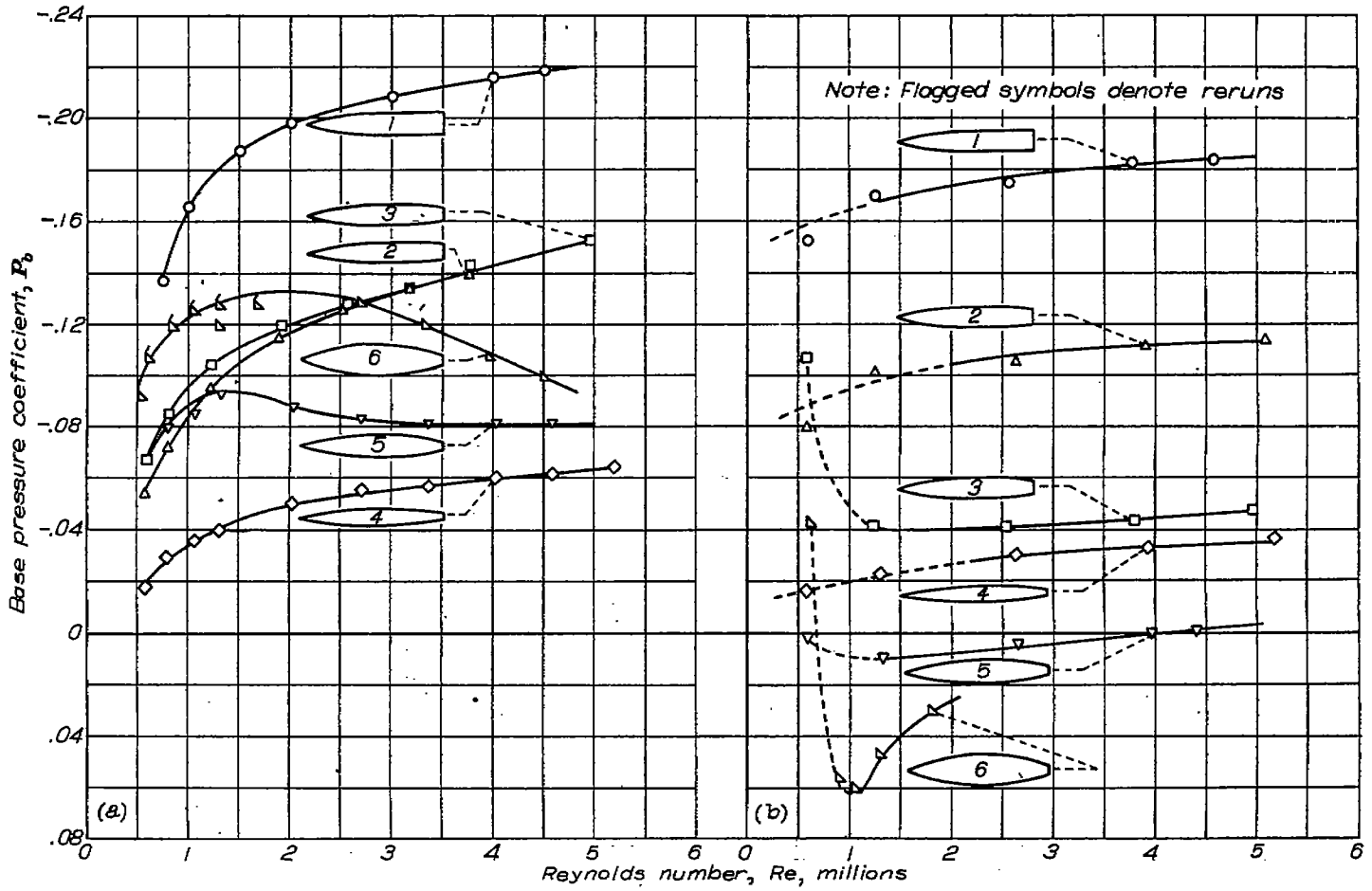

(a) Smooth condition. (b) Roughness added.

FIGURE 26.—Variation of base-pressure coefficient with Reynolds number for models 1, 2, 3, 4, 5 and 6 in the smooth condition and with roughness added.

consequent increase in the pressure drag of the boattail. For model 1, which has no boattailing, the increase in skin friction is the sole factor contributing to the increase in foredrag.

Base pressure and base drag.—Figure 26 (a) shows the base pressure coefficients plotted as a function of the Reynolds number for models 1 through 6, each with a smooth surface. It is evident from the data in this figure that the effects of Reynolds number on base pressure for a body with a laminar boundary layer are quite large. In the range of Reynolds numbers covered, the base pressure coefficient of model 1 increases about 60 percent, and the coefficients of models 2, 3, and 4 more than double. The thicker bodies with boattailing, models 5 and 6, do not exhibit such large changes in base pressure coefficient, for the coefficients apparently reach a maximum at a relatively low Reynolds number, and then decrease with further increase in the Reynolds number.

The base pressure coefficients for models 1 through 6 with roughness added are shown in figure 26 (b). Here again, the portions of the curves which correspond to the low Reynolds number region wherein transition was not completely effected are shown as dotted lines. Model 1 exhibits the lowest base pressure and model 6 the highest; in this latter case the base pressure is even higher than the free-stream static pressure. The physical reason for this is evident from the schlieren photograph at the bottom of figure 20, which shows that a compression through the shock wave occurs just ahead of the base of model 6. Except for the large changes in pressure coefficient at low Reynolds numbers where the desired transition was not effected, the variation of base pressure coefficient with Reynolds number is relatively small for the bodies with roughness added.

From a comparison of the curves for the bodies with roughness added to the corresponding curves for the smooth-surfaced bodies, it is evident that a large change in the base pressure coefficient is attributable to the change in the condition of the boundary layer. In general, the base pressures for bodies with roughness added are considerably higher than the corresponding base pressures for the smooth-surfaced bodies. In the case of the boattailed bodies the physical reason for this increase in the base pressure is the appearance of the base shock wave, as shown in figure 21. For model 1, which has no boattailing, the mixing action and greater thickness of the turbulent boundary layer are probably responsible for the observed increase.

The foregoing data show that the effects of Reynolds number and condition of the boundary layer on the base pressure of a body moving at supersonic speeds depend considerably upon the shape of the afterbody. In order to ascertain whether the effects of viscosity also depend upon the length-diameter ratio for a fixed shape of afterbody, some models of different length-diameter ratios were tested and the data presented in figures 27 (a) and 27 (b) which show the variation of base pressure coefficient with Reynolds number. The data presented in this figure are not free of

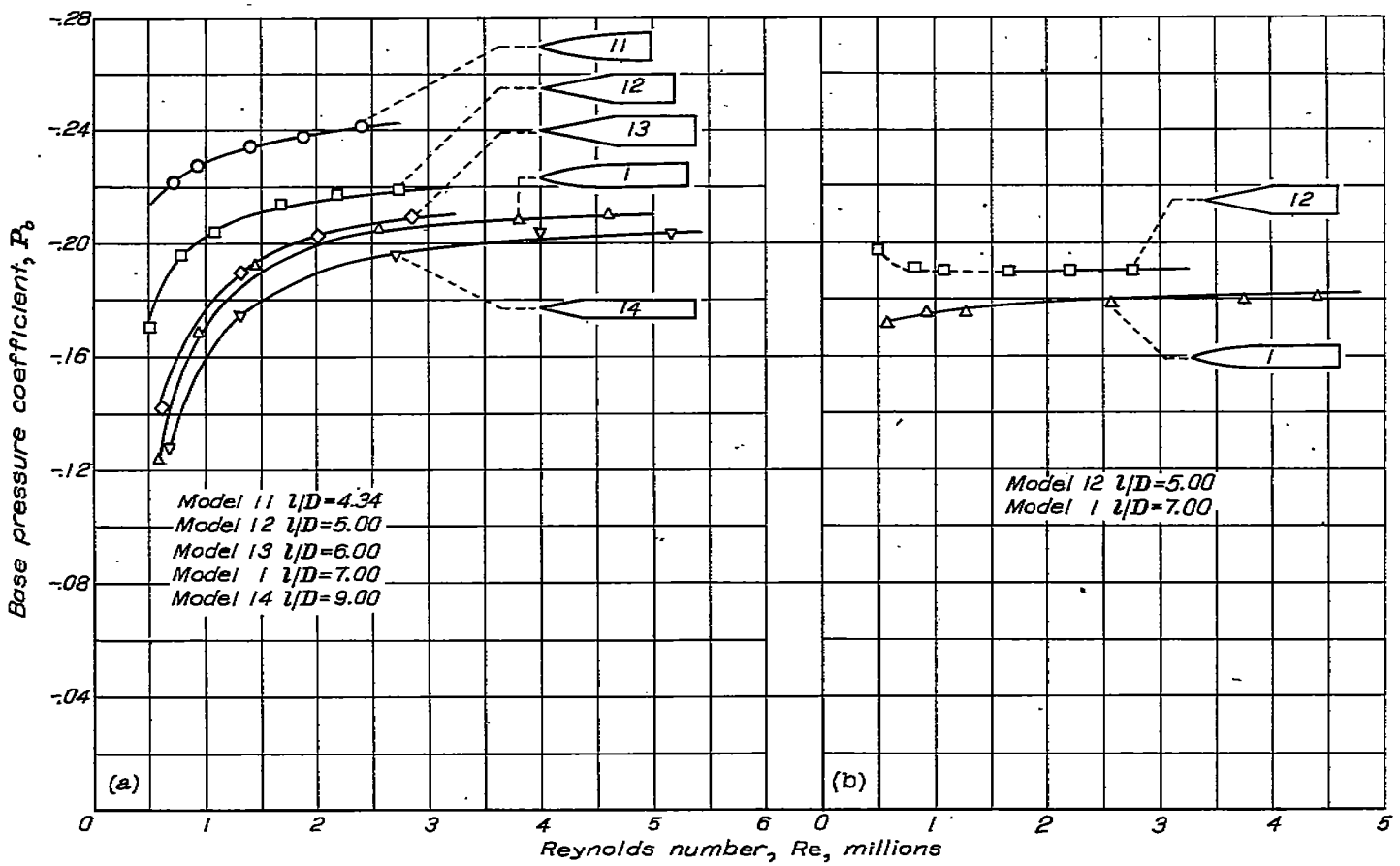

(a) Smooth condition. (b) Roughness added.

FIGURE 27.—Variation of base-pressure coefficient with Reynolds number for bodies without boattailing but with different length-diameter ratios.

support interference. From these data it is apparent that the effects of viscosity on the base pressure increase with the length-diameter ratio of the body.[5] It is to be noted that the base pressure increases as the length-diameter ratio increases. This is somewhat at variance with the results of reference 20, which showed an effect, but not a systematic one, of length-diameter ratio on the base pressure of bodies without boattailing.

The base drag coefficient can be obtained from the base pressure coefficient of the models by using equation (2). The base drag coefficients for the smooth-surfaced bodies are presented in figure 28 (a) and for the bodies with roughness added in figure 28 (b). These curves are, of course, similar to the corresponding curves of base pressure coefficient given in figures 26 (a) and 26 (b). In this form the ordinates can be added directly to the foredrag coefficients of figure 23 to obtain the total drag coefficient of a given body. It is seen that the contribution of the base pressure to the total drag is very small for models with large amounts of boattailing, such as models 3, 4, 5, and 6.

Total drag.—The total drag coefficients for models 1 through 6 with smooth surfaces are shown in figure 29 (a) as a function of Reynolds number. These data show that the drag coefficients of both models 1 and 2 with a laminar boundary layer increase a little over 20 percent from the lowest to the highest value of Reynolds number obtained in the tests. The other models exhibit somewhat smaller changes. The data presented in figures 23 and 28 indicate that the principal effect controlling the variation of total drag with Reynolds number for laminar flow in the boundary layer is the effect of Reynolds number on the base drag of the bodies. For the special case of highly boattailed bodies, however, this effect is of little relative importance because the base drag is a small part of the total drag. In such cases, the over-all variation of drag coefficient is due almost entirely to the variation of foredrag with Reynolds number.

Figure 29 (b) shows the total drag coefficients plotted as a function of the Reynolds number for models 1 through 6 with roughness added. Again, the portions of the curves that are shown dotted represent the Reynolds number region in which the amount of roughness added is insufficient to cause complete transition. All the curves have approximately the same trend, the over-all effect on the drag coefficients being about 15 percent or less for the various bodies.

A comparison of the curves of total drag for bodies with roughness added to the corresponding curves for bodies with smooth surfaces shows an interesting phenomenon. At the higher Reynolds numbers the drag of models 1 and 6 is actually decreased slightly by the addition of roughness, in spite of the corresponding increase in skin-friction drag. The reason is, of course, that the base drags are very much

[5] Similar experiments conducted at a Mach number of 2.0 have shown the same trend. Both sets of data show reasonable correlation with the ratio of boundary-layer thickness to base diameter.

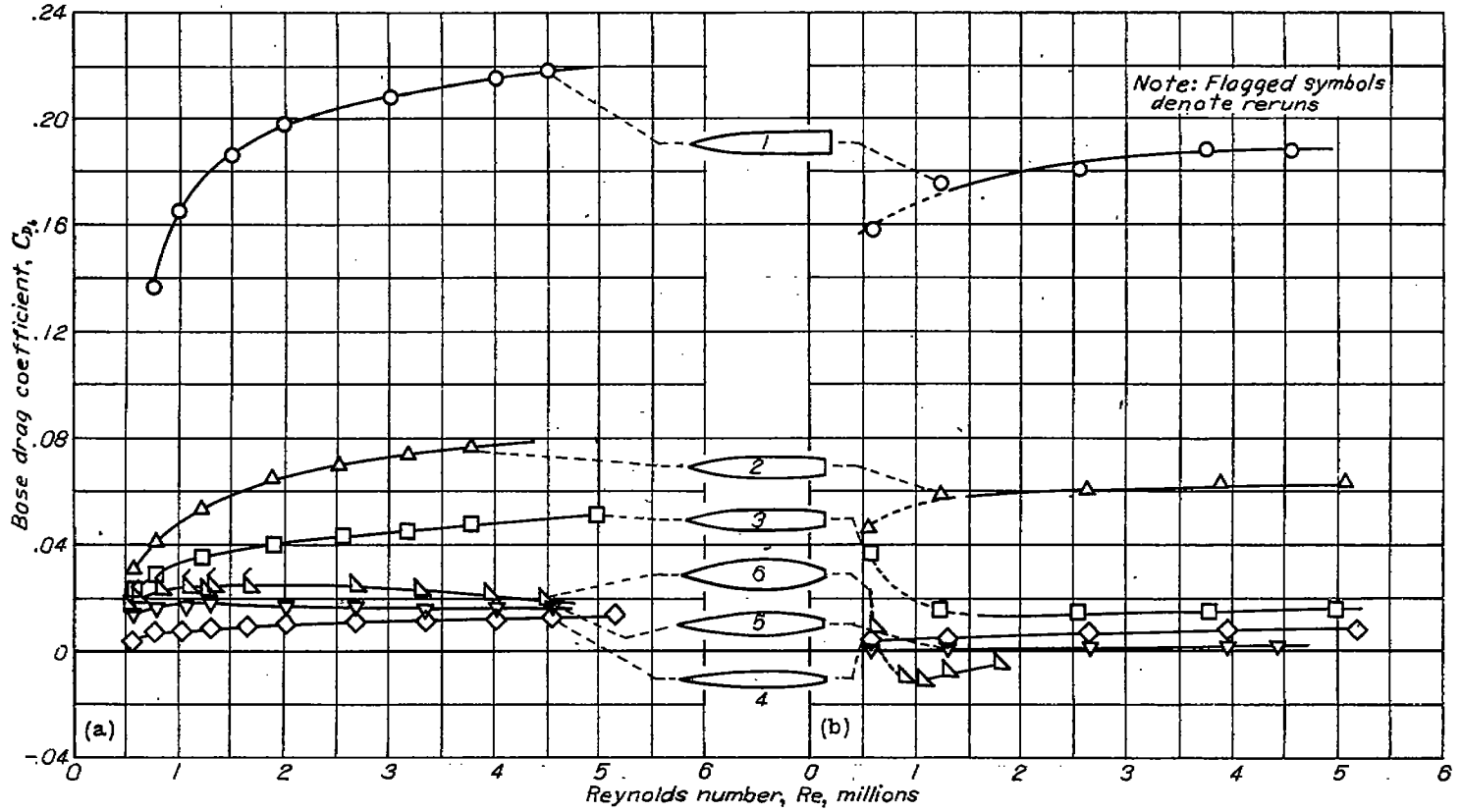

(a) Smooth condition. (b) Roughness added.

FIGURE 28.—Variation of base-drag coefficient with Reynolds number for models 1, 2, 3, 4, 5 and 6 in the smooth condition and with roughness added.

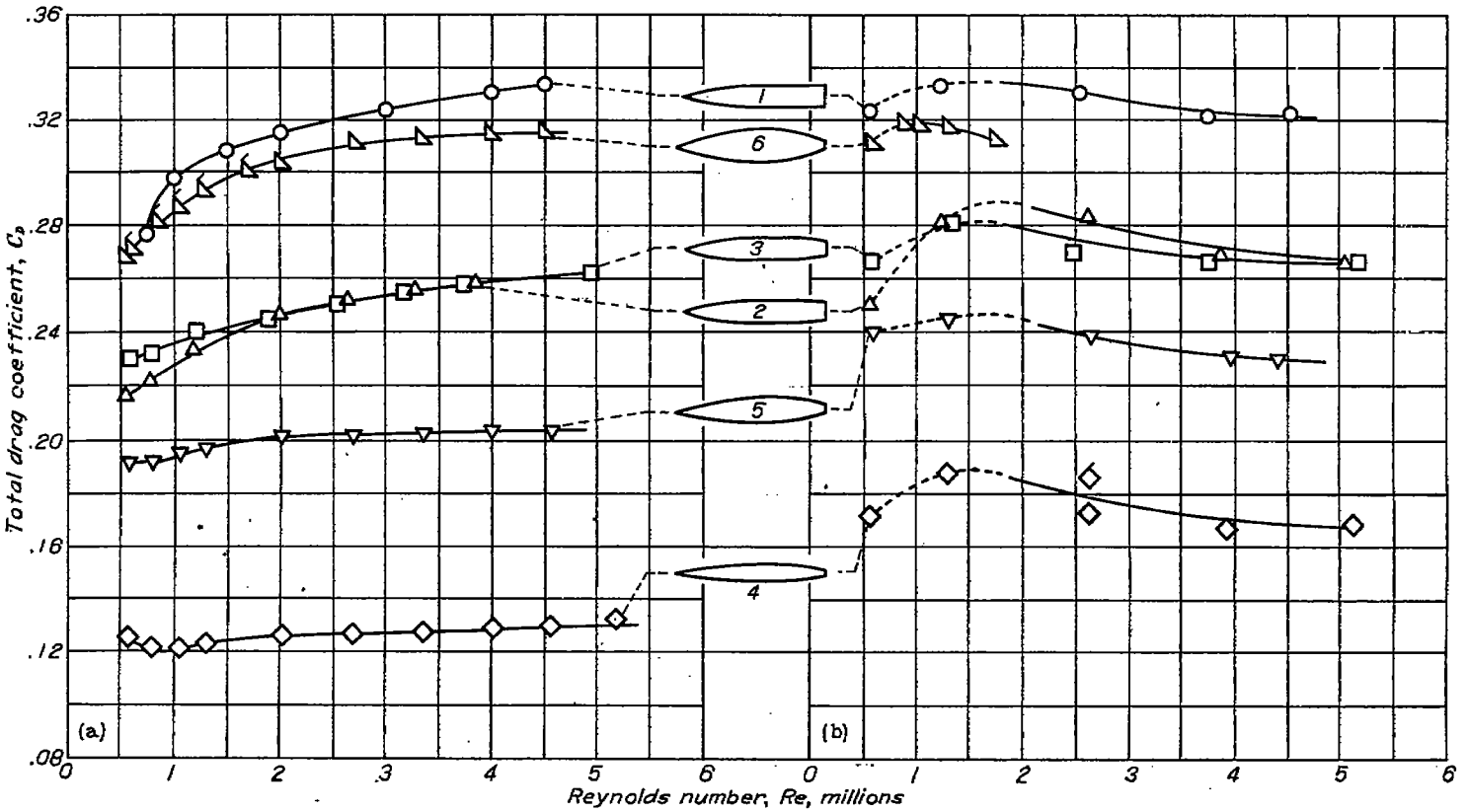

(a) Smooth condition. (b) Roughness added.

FIGURE 29.—Variation of total drag coefficient with Reynolds number for models 1, 2, 3, 4, 5 and 6 in the smooth condition and with roughness added.

lower for the turbulent boundary layer than for the laminar. The drag coefficients of the other bodies (models 2, 3, 4, and 5) are somewhat higher with roughness added, because the increase in friction drag of the turbulent boundary layer is greater than the decrease in base drag.

The importance of always considering both the Reynolds number of the flow and condition of the boundary layer is illustrated by the total drag characteristics of model 2. For example, if model 2 were tested with a turbulent boundary layer at a Reynolds number of 2×10^6, the drag would be about 35 percent higher than if tested with a laminar boundary layer at a Reynolds number of 0.5×10^6. Although discrepancies as large as these have not been reported as yet in the drag data from different supersonic wind tunnels, certain consistent differences, varying from about 5 to 25 percent, have been reported (reference 18) in the drag data of similar projectiles tested in the Gottingen and the Kochel tunnels. Although in reference 18 the discrepancies between the two tunnels were attributed only to the variation in skin friction with Reynolds number, it appears from the results of the present investigation that such discrepancies are attributable primarily to differences in flow separation and base pressure.

A comparison of the effects of viscosity for pointed bodies with the effects for a blunt body shows clearly that body shape must be considered, and that conclusions about viscosity effects based upon tests of blunt bodies may be completely inapplicable to the aerodynamic shapes which are suitable for supersonic flight. For example, in the case of a sphere at 1.5 Mach number with an over-all Reynolds number variation of from 7.5×10^4 to 9.0×10^5, the agreement between the drag data from Gottingen (reference 7), Peenemunde (reference 18), and the present wind tunnel is within 1 percent of the values measured for free-flight (references 7 and 21). It is evident that the effects of viscosity on the drag of a sphere are quite different from the effects on the pointed bodies tested in this investigation.

CONCLUSIONS

The conclusions which follow apply for a Mach number of 1.5 and at Reynolds numbers based upon model length up to about 5×10^6 for bodies of revolution similar to the ones tested.

1. The effects of viscosity differ greatly for laminar and turbulent flow in the boundary layer, and within each regime depend upon the Reynolds number of the flow and the shape of the body.

2. Laminar flow was found on the smooth bodies up to a Reynolds number of 6.5×10^6 and may possibly exist to considerably higher values.

3. A comparison between the test results for laminar and for turbulent flow in the boundary layer at a fixed value of the Reynolds number shows that:

(a) The resistance to separation with turbulent flow in the boundary layer is much greater.

(b) The shock-wave configuration near the base of boattailed bodies is markedly different for the two types of boundary layer flow.

(c) The foredrag coefficients with turbulent boundary layer ordinarily are higher.

(d) The base pressure on boattailed bodies is much higher with the turbulent boundary layer.

(e) The total drag is usually higher with the turbulent boundary layer.

4. For laminar flow in the boundary layer the following effects were found:

(a) The laminar boundary layer separates forward of the base on all boattailed bodies tested, and the position of separation varies noticeably with Reynolds number. Laminar separation is not necessarily accompanied by a shock wave originating from the point of separation. On many of the models the pressure in an inviscid flow would continually decrease in the direction of the flow upstream of the separation point.

(b) The trailing shock wave moves forward slightly as the Reynolds number is increased, but no significant change takes place in the shock-wave configuration near the base.

(c) With increasing Reynolds numbers, the foredrag coefficients increase for highly boattailed bodies and decrease for bodies without boattailing. For moderately boattailed bodies the variation of the foredrag coefficient with Reynolds number is relatively small.

(d) The base pressure changes markedly with Reynolds number. For bodies with the same afterbody shape, the base pressure also depends upon the length-diameter ratio of the body.

(e) Total drag varies considerably with the Reynolds number, changing more than 20 percent for several of the models.

5. For turbulent flow in the boundary the following effects were found:

(a) Separation does not ordinarily occur upstream of the base except for highly boattailed bodies.

(b) The shock-wave configuration near the base does not change noticeably as the Reynolds number changes.

(c) The foredrag coefficients decrease slightly as the Reynolds number is increased.

(d) The base pressure changes very little with changing Reynolds number.

(e) The total drag decreases as the Reynolds number is increased.

AMES AERONAUTICAL LABORATORY,
NATIONAL ADVISORY COMMITTEE FOR AERONAUTICS,
MOFFETT FIELD, CALIF., *January 31, 1947.*

213637—53——53

APPENDIX A

VARIATION OF TEST-SECTION STATIC PRESSURE

Since the static pressure with no model present varied along the axis of the test section as shown in figure 5, it was necessary to apply a correction to the measured coefficients to account for the increment in drag or pressure resulting from this axial pressure gradient. Although the axial variation of test-section static pressure is not monotonic, the pressures at the downstream end of the test section are uniformly lower than the pressures of the upstream end where the nose of a model is ordinarily placed. This means that the actual pressure exerted at a given point on a body is lower than it would be if the ambient pressure gradient were zero as it is in free flight. The gradient corrections are calculated on the assumption that the magnitude of the pressure exerted at an arbitrary point on the body in the tunnel is lower than it would be if no gradient were present by an increment equal to the amount which the static pressure decreases (with no model present) from the position of the model nose to the position of the arbitrary point. At the Mach number of the present tests it is not necessary to include the corresponding axial variation of dynamic pressure in the corrections since it varies only ± 0.2 percent from the mean test-section value used in all calculations. The corrections to the measured coefficients of model 1 located 2.5 inches downstream from the reference pressure orifice, for example, amount to ± 0.012 in foredrag coefficient and -0.026 in base-drag coefficient; the corresponding percentages of the uncorrected coefficients of foredrag and base pressure are 12 and 15, respectively.

Because the gradient correction is relatively large in the present tests an experimental justification of such theoretical corrections is in order. The validity of the corrections as applied to foredrag is confirmed by tests on model 9, which consists of a conical nose with a 20° included angle and a short cylindrical afterbody. The theoretical foredrag of this body, which is equal to the sum of the wave and friction drags can be easily determined as a function of Reynolds number. The wave drag of the conical nose is given by the calculations of Taylor and Maccoll (references 10 and 11). The frictional drag can be estimated using the low-speed laminar skin-friction coefficients, since the boundary layer was completely laminar over this model. A comparison of the corrected and uncorrected foredrag with the theoretical foredrag is shown in figure 6. The corrected foredrag coefficients are seen to be in good agreement with the theoretical values; whereas the uncorrected data fall below the wave drag at high tunnel pressures. This latter condition, of course, represents an impossible situation for a body without boattailing.

In order to check experimentally the validity of the corrections as applied to the measured base pressure, model 1 was tested on the side support at five different positions along the axis of the test section. Because the support system remained fixed relative to the body, the interference of the support is the same in each case, hence, any discrepancies in the measured base pressures at the various positions are attributable only to the pressure gradient along the tunnel axis. Figure 7 shows that the uncorrected base pressure data taken at the five different positions differ by about 25 percent, but the corresponding five sets of corrected data fall within about ± 1.5 percent of their mean, thus confirming the validity of the correction.

APPENDIX B

PRECISION OF DATA

The accuracy of the results presented can be estimated by considering the possible errors that are known to be involved in the measurement of the forces and pressures, and in the determination of the free-stream Mach number and gradient corrections.

The force measurements are subject to errors from shifts in the balance zero due to temperature effects and also from a shift in the calibration constant. The zero shift, which is less than ± 1 percent of the force data at low pressures and less than ± 0.2 percent at high pressures, was checked periodically by running the tunnel through the complete temperature range with no force applied to the balance. In the majority of cases the variation of the balance calibration constant, which was checked before and after each series of tests, permitted a possible deviation of ± 0.3 percent in the force data. All data presented in figures 9 (b), 13, 14, and the data for models 4, 5, and 6 in figures 23 (a) and 29 (a) were obtained during a period between two consecutive balance calibrations for which the constant differed by 6.4 percent. A comparison of the data obtained during this period with theoretical results and with the results of subsequent reruns of some of the same models indicates that the change in balance calibration occurred before the data in question were obtained. The results in the afore-mentioned figures were therefore computed on the basis of the later calibration. It is estimated that the maximum error in the balance calibration constant for these results is at worst no greater than $+0.3$ to -3.0 percent.

The pressure data, including the dynamic pressure, are subject to small errors resulting from possible inexact readings of the mercury manometers. The base pressure data are also subject to an additional error resulting from the small variation in the specific gravity of the dibutyl phthalate indicating fluid. At the most, these sources can cause an error in the total and foredrag coefficients of about ± 0.3 percent, and in the base-drag coefficient of about ± 0.8 percent. The error in dynamic pressure due to the uncertainty in the free-stream Mach number is negligible, since the isentropic relation for the dynamic pressure as a function of Mach number is near a maximum at a Mach number of 1.5. For slender bodies of revolution the variation of the force coefficients with Mach number is quite small; hence, errors resulting from the variation of free-stream Mach number from 1.49 to 1.51 are negligible.

On the basis of the data presented in figures 6 and 7, it is estimated that for all tunnel pressures the uncertainty in the gradient corrections to total drag, foredrag, and base pressure coefficients can cause at the most an error in these coefficients of ± 0.004, ± 0.004, and ± 0.005, respectively. It should be noted that in the table on precision, presented in the section on results, this source of error, which is independent of tunnel pressure, is expressed as an increment and not as a percentage of the measured coefficient.

Previous investigations have shown that an uncertainty may be introduced in supersonic wind-tunnel data if the humidity of the tunnel air is very high. To determine the effects of this variable in the present investigation, the specific humidity was varied from the lowest values (approximately 0.0001) to values approximately 20 times those normally encountered in the tests. Drag and base pressure measurements were taken on a body with a conical head and also on a sphere. The results showed no appreciable effect of humidity over a range much greater than that encountered in the present tests, provided the variation in test-section dynamic pressure with the change in humidity was taken into account in the reduction of the data. It is believed, therefore, that the precision of the results presented in this report is unaffected by humidity.

APPENDIX C

EFFECT OF SUPPORT INTERFERENCE

A knowledge of the effects of support interference upon the data in question is essential to an understanding of its applicability to free-flight conditions. Previous to the present investigation an extensive series of tests were conducted to determine the body shape and support combinations necessary to evaluate the support interference.

In general, it was found that for the models tested in the smooth condition (laminar boundary layer) the effect of the rear supports used in the present investigation was negligible for the boattailed models 2 and 3 and was appreciable only in the base pressure measurements for model 1. For model 1, combinations of rear support and side support were used to evaluate the effect of the rear support on the base pressure. The evaluation was made on the assumption of no mutual interference between the rear support and side support and was checked by the use of two different combinations of side support and rear support. The data indicate that the assumption is justified within the limits of the experimental accuracy and that the corrected, interference-free base pressures deduced by this method differ only slightly from those measured with the side support alone.

For the bodies with roughness added (producing a turbulent boundary layer) a complete investigation of the support interference was not made; consequently, a definite quantitative evaluation of the interference effects for each body in this condition cannot be given. From the data that were obtained it has been found that the foredrag is not affected appreciably by the presence of the supports used in the present investigation, but that a small amount of interference is evident in the base pressure coefficient which may vary from a minimum of ± 0.005 to a maximum of ± 0.015 for the different bodies. This uncertainty in the base pressure coefficient results in a correspondingly small uncertainty in the base drag coefficient and in the total drag coefficient.

REFERENCES

1. Ackeret, J., Feldmann, F., and Rott, N.: Investigations of Compression Shocks and Boundary Layers in Gases Moving at High Speed. NACA TM 1113, 1947.
2. Liepmann, H. W.: Further Investigations of the Interaction of Boundary Layer and Shock Waves in Transonic Flow. Jour. Aero. Sci., vol. 13, no. 12, Dec. 1946, pp. 623–637.
3. Theodorsen, Theodore, and Regier, Arthur: Experiments on Drag of Revolving Disks, Cylinders and Streamline Rods at High Speeds. NACA Rep. 793, 1944. (Formerly NACA ACR L4F16)
4. Keenan, Joseph H., and Neumann, Ernest P.: Friction in Pipes at Supersonic and Subsonic Velocities. NACA TN 963, 1945.
5. Frössel, W.: Flow in Smooth Straight Pipes at Velocities Above and Below Sound Velocity. NACA TM 844, 1938.
6. Ferri, Antonio: Influenza del Numero di Reynolds ai Grandi Numeri di Mach. Ministero del Aeronautica, Direzione Superiore Studi e delle Esperienze, Atti di Guidonia N. 67–68–69, Mar. 10, 1942, pp. 49–92.
7. Walchner, O.: Systematische Geschossmessungen im Windkanal. Lilienthal-Gesellschaft für Luftfahrtforschung, Bericht 139, Teil 1, Oct. 1941, pp. 29–37. (Available as NACA TM 1122)
8. Bach, F.: Druckverteilungsmessungen an Geschossmodellen. Zentrale für Wissenschaftliches Berichtswesen der Luftfahrtforschung, Berlin-Adlershof. UM 6057, Mar. 1945.
9. Van Dyke, Milton D.: Aerodynamic Characteristics Including Scale Effect of Several Wings and Bodies Alone and in Combination at a Mach Number of 1.53. NACA RM A6K22, 1946.
10. Maccoll, J. W.: The Conical Shock Wave Formed by a Cone Moving at a High Speed. Proc. of the Royal Soc. of London, Ser. A, Vol. 159, Apr. 1, 1937, pp. 459–472.
11. Taylor, G. I., and Maccoll, J. W.: The Air Pressure on a Cone Moving at High Speeds. Proc. of the Royal Soc. of London, Ser. A, Vol. 139, Feb. 1, 1933, pp. 278–311.
12. Sauer, R.: Charakteristikenverfahren für Räumliche Achsensymmetrische Überschallstromungen. Zentrale für Wissenschaftliches Berichtswesen, Berlin, F. B. No. 1269, Aug. 14, 1940. (Available as NACA TM 1133)
13. Sauer, R.: Theoretische Einführung in die Gasdynamik. Berlin, Springer, 1943. (Reprinted by Edwards Bros., Ann Arbor, Mich., 1945.)
14. Tollmein, W., and Schäfer, M.: Rotationssymmetrische Überschallstromungen. Lilienthal-Gesellschaft für Luftfahrtforschung, Bericht 139, Teil 2, Oct. 1941, pp. 5–15.
15. Allen, H. Julian, and Nitzberg, Gerald E.: The Effect of Compressibility on the Growth of the Laminar Boundary Layer on Low-Drag Wings and Bodies. NACA TN 1255, 1947.
16. Matt, H.: Hochgeschwindigkeitsmessungen an Rund-und Profilstangen verschiedener Durchmesser. Lilienthal-Gesellschaft für Luftfahrtforschung, Bericht 156, Oct. 1942, pp. 109–113.
17. Lees, Lester: The Stability of the Laminar Boundary Layer in a Compressible Fluid. NACA Rep. 876, 1947. (Formerly NACA TN 1860)
18. Lehnert, R.: Systematische Messungen an neun einfachen Geschossformen im Vergleich zu Messungen der AVA-Göttingen. Lilienthal-Gesellschaft für Luftfahrtforschung, Bericht 139, Teil 2, 1941, pp. 31–34.
19. Ferri, Antonio: Experimental Results with Airfoils Tested in the High-Speed Tunnel at Guidonia. NACA TM 946, 1940.
20. Erdmann, S.: Widerstandsbestimmung Von Kegeln und Kugeln aus der Druckverteilung bei Überschallgeschwindigkeit. Lilienthal-Gesellschaft für Luftfahrtforschung, Bericht 139, Teil 2, Oct. 1941.
21. Charters, A. C., and Thomas, R. N.: The Aerodynamic Performance of Small Spheres from Subsonic to High Supersonic Velocities. Jour. Aero. Sci., vol. 12, No. 4, Oct. 1945, pp. 468–476.